Impact of tectonic rafts' gravitational instability on fault reactivation and geometry

Abubakar Maunde[a, b, *], Tiago M. Alves[a]

[a] 3D Seismic Lab, School of Earth and Ocean Sciences, Cardiff University, Main Building, Park Place, Cardiff, CF10 3AT, United Kingdom

[b] Geology Department, School of Physical Sciences, Modibbo Adama University of Technology, P.M.B 2076, Yola, Nigeria

***Corresponding author**: E-mail: abubakarmaunde@yahoo.co.uk; maundea@cardiff.ac.uk Telephone: +2348161358265; +447778942870

Abstract

Downslope gravitational instability of tectonic rafts has been identified as deforming large volumes of post-salt strata on the passive continental margins. Detailed mapping of fault throw and geometry using three-dimensional (3D) seismic reflection data from the salt-rich Espírito Santo Basin (SE Brazil) shows that the complex fault geometries observed are primarily a function of downslope gravitational instability of tectonic rafts. Three main tiers of faults were identified and their geometry analysed in detail. Tier 1 faults are associated with the initial stage of fragmentation of post-salt strata into individual blocks, or rafts, which are separated by listric (roller) faults and associated minibasins. These faults comprise closely spaced set of normal faults that resulted from outer-arc stretching of strata overlaying discrete tectonic rafts. The faults accommodate a significant part of the bending strain occurring in the hanging-wall blocks of roller faults, thus forming a curved-polygonal planform geometry adjacent to large roller faults. Tier 2 faults are associated with a renewed stage of downslope gravitational gliding of tectonic rafts. The progressive bending of overburden strata during this stage led to the progressive faulting of overburden strata by these faults. The faults comprise closely spaced normal faults with a restricted range in fault strikes, forming a rectangular-polygonal planform geometry over rollover anticlines. Tier 3 faults are associated with a later stage of diachronous grounding of tectonic rafts. Differences in the degree of diachronous grounding of tectonic rafts are responsible for the development of these faults and subsequent shortening of the overburden strata. These faults comprise densely spaced set of normal faults with diverse range of fault strikes, forming an irregular-polygonal planform geometry over rollover anticlines. The interpreted fault tiers show fault throw maxima ranging from 50 m to 60 m, spacings of 180-420 m and trace lengths of 120-650 m. The interpreted fault tiers were reactivated and their growth is characterized by fault segment linkage. The diachronous downslope translation and grounding (welding) of the tectonic rafts on pre-salt strata was an important process controlling the degree of deformation off Espírito Santo. Successive episodes of fault reactivation, and the subsequent generation of salt welds below tectonic rafts, potentially formed large conduits favouring fluid migration and the generation of hydrocarbon traps in supra-salt strata.

Keywords: Tectonic rafts; gravitational gliding; fault reactivation; fault geometry; rollover anticlines.

1. Introduction

The proximal continental slopes of salt-rich continental margins, such as offshore Angola–Congo and southeast Brazil, are characterised by large-scale withdrawal and downslope movement of salt under deltaic wedges (Demercian et al., 1993; Cramez and Jackson, 2000; Fort et al., 2004; Alves et al., 2009). This process triggers gravitational instability and has led, in the past, to the fragmentation of supra-salt strata into individual blocks, or rafts, separated by listric (roller)

faults and associated minibasins. At places, these fragmented blocks of strata (rafts) are overlain by wide rollover anticlines (Duval et al., 1992; Cramez and Jackson, 2000; Alves, 2012). Importantly, the continuous downslope translation and grounding of rafts above pre-salt units have induced a continuum of overburden deformational styles not only in southeast Brazil, but through vast areas of West Africa (Duval et al., 1992; Gaullier et al., 1993; Mauduit et al., 1997; Penge et al., 1999; Alves, 2012; Pilcher et al., 2014). It also led to: a) significant subsidence in extensional basins located updip from moving rafts, b) the development of large listric (roller) faults controlling seafloor topography during supra-salt extension, c) the development of growth strata infilling the accommodation spaces created by raft movement, and d) the development of reactivated structures, which at places developed into pop-up structures and wide rollover anticlines sub-parallel to the strike of individual rafts (Alves, 2012).

In the continental margin of southeast Brazil, deformation driven by the gravitational gliding of rafts has been a relatively continuous process. Local tectonic shortening began early after the deposition of post-salt strata and continued unabated up to the present day. However, individual rafts ceased movement at different times depending on their geometry, salt supply and overburden thickness (Fiduk et al., 2004; Alves, 2012; Piedade and Alves, 2017). Earlier studies on tectonic rafts considered that differences in supra-salt overburden thickness can maintain downslope gravitational gliding of rafts even if slope gradient is close to zero, as long as an efficient basal décollement is present at depth (Duval et al., 1992; Gaullier et al., 1993; Mauduit et al., 1997; Vendeville, 2005; Brun and Mauduit, 2009). Such a story of gravitational gliding of rafts will be potentially recorded by rollover faults geometry, wide rollover anticlines, stratal shortening and associated salt structures. For instance, Alves (2012) reported that distinct tectonic episodes of gravitational gliding of rafts controlled the Late Cretaceous-Paleogene evolution of the basin, inducing local shortening, wide rollover anticlines and fault reactivation.

Fault reactivation has been described as reflecting the further propagation of pre-existing faults after a significant period of quiescence (e.g. Cartwright et al., 1995; Mansfield and Cartwright, 2001; Peacock and Sanderson, 1991; Baudon and Cartwright, 2008). The classical model for fault reactivation assumes upward propagation from pre-existing structures as faults are generated at depth (Richard and Krantz, 1991). The early fault growth model of Barnett et al. (1987) initially favoured the development of isolated normal faults propagating in a radial direction, and records no migration of maximum displacement points. Recent work has focused on documenting changes in the dimensions and absolute fault displacements to build more reliable fault-propagation models (e.g. Cartwright et al., 1995; Mansfield and Cartwright, 2001, 1996; Cartwright and Mansfield, 1998). It is now recognised that larger faults are a result of fault-segment linkage associated with propagation in both the vertical and horizontal directions (Cartwright et al., 1995; Mansfield and Cartwright, 2001; Peacock and Sanderson, 1991; Dawers and Anders, 1995). Morley (1999) argued for an early linkage of multiple smaller faults, rather than growth following the isolated fault model. A supplementary model has been presented by Lohr et al. (2008), who demonstrated that most faults grown by the coalescence of multiple smaller fault segments, whereas tip propagation is of relatively minor importance. Acknowledging this latter process of fault growth, Cartwright et al. (2000) and McLeod et al. (2000) defended that the geometry of large faults is essentially controlled by existing small fault segments.

This work aims at understanding the effect of gravitational gliding of rafts on fault reactivation and geometry over rollover anticlines developed above tectonic rafts. Using a high quality 3D seismic dataset from the Espírito Santo Basin, offshore southeast Brazil we extrapolate our results to other salt-rich continental margins where similar phenomena have occurred (e.g. offshore Angola-Congo, North Sea; e.g. Duval et al., 1992; Mauduit et al., 1997; Cramez and Jackson, 2000). Thus, this study aims to address the following questions:

a. How are faults over rollover anticlines reactivated in areas dominated by raft tectonics?
b. Does the geometry of faults over rollover anticlines document discrete episodes of gravitational gliding?
c. What are the modes of fault propagation developing during the gravitational gliding in tectonic rafts?

To simplify the analysis in this study, we mapped eight age-constrained stratigraphic unconformities in both the Cretaceous and Cenozoic strata (Fig. 2). These unconformities truncate the interpreted fault families, thus allowing for the relatively dating of fault movement below and above them (Fig. 2). We further assessed fault growth histories through the collection of fault displacement data (e.g. Peacock and Sanderson, 1991; Cartwright and Mansfield, 1998; Mansfield and Cartwright, 2001; Stewart, 2001; Morley, 2002; Peacock, 2002; Baudon and Cartwright, 2008; Zhang et al., 2011; Anette et al., 2013). Throw-depth (T-Z) plots offer information on the nucleation, propagation, segmentation and linkage of individual faults, providing at the same time important data for fault seal prediction (Stewart, 2001; Koledoye et al., 2003; Faulkner et al., 2010). In parallel, throw gradients have been used to assess the role of lithology and tectonic reactivation on the growth of faults (Cartwright and Mansfield, 1998; Baudon and Cartwright, 2008), as discrepancies in throw gradients commonly result from mechanical heterogeneities, fault linkage and fault segmentation (Baudon and Cartwright, 2008).

2. Geological setting

The Espírito Santo Basin is located on the continental margin of southeast Brazilian (Fig. 1). The basin covers an area of about 125,000 km^2, of which 18,000 km^2 are onshore and 107, 000 km^2 are offshore (Fiduk et al., 2004). It is associated with the continental break-up of Gondwana, which lasted from the Late Jurassic to Early Cretaceous, and subsequent opening of the South Atlantic Ocean (Chang et al., 1992; Davison, 1999; Meisling et al., 2001). The Espírito Santo Basin shares a very similar geological history to other basins from southeast Brazil (e.g. Campos and Santos basins); all have accumulated a very thick stratigraphic succession that includes lithologies as variable as basalt flows in the pre-rift sequence, continental sandstones and shales in the rift sequence, carbonate and evaporites in the transitional sequence, and deep-marine siliciclastic and carbonate sediments in the post-rift sequence (Bruhn and Walker, 1997; Mohriak et al., 1998). The Espírito Santo Basin is limited to the north by the Early to Middle Eocene volcanic Abrolhos Plateau and to the south by the Vitória High, which separates it from the Campos Basin (Guardado et al., 1989; Bruhn and Walker, 1997; Fiduk et al., 2004; Alves et al., 2009; Alves, 2012) (Fig. 1).

The geodynamic evolution of the Espírito Santo Basin was primarily controlled by four tectonic stages, which were also common along most South Atlantic continental margins: the pre-rift, syn-rift, transitional and drift stages (Ojeda, 1982; Mohriak et al., 1998; Gibbs et at., 2003) (Fig. 2). Mohriak et al. (1998) correlated these tectonic stages with three main depositional megasequences: 1) a pre-rift megasequence (Late Jurassic to Earliest Cretaceous) dominated by extrusive magmas, volcaniclastic material and tuffs deposited unconformably over a Pre-Cambrian basement (Asmus et al., 1971); 2) a syn-rift megasequence (Berriasian to Early Aptian), with continental sandstones, silts and shales, together with fault-related syn-tectonic conglomerates and basaltic volcaniclastic rocks (Ojeda, 1982, Mohriak et al., 1998; Gamboa et al., 2010; Chang et al., 1992); and 3) the post-rift megasequence (Aptian to Recent), the main interval of interest of this study, which is subdivided into three sequences - transitional, early drift transgressive marine, and late drift regressive marine (Fig. 2).

The transitional sequence (Unit S2; Mid Aptian to Early Albian) comprises thick layers of evaporitic sediments separated from the syn-rift Unit S1 by an angular unconformity of regional expression (Ojeda, 1982; Chang et al., 1992; Demercian et al., 1993; Davison, 1999; Mohriak et al., 1995). Salt structures in this sequence show a proximal to basinward transition from salt rollers to vertical diapirs (Fig. 3). The transitional stage in southeast Brazil records the deposition of >3000 m of

evaporites, mainly halite and anhydrite resulting from extreme marine evaporation in arid climatic conditions (França et al., 2007; Mohriak, 2003; Mohriak et al., 2008). The end of the transitional cycle is marked by the onset of extrusive igneous activity related to a newly-formed oceanic spreading ridge (Mohriak et al., 2008; Ojeda, 1982; Davison, 1999, 2007).

The early drift sequence (Albian to Early Eocene), which follows the transitional sequence, represents two marine-transgressive sequences (Units S3 and S4; Fig. 2), with a shallow-water carbonate platform developing from the late Albian to Cenomanian (Chang et al., 1992). The onset of this carbonate platform is documented by the São Mateus and Regência Formations, which were deposited over the Itaúnas Member evaporitic sequence (Mohriak, 2003; França et al., 2007) (Fig. 2). The São Mateus Formation consists of sandstones deposited in a proximal marine setting over a succession of shales, siltstones, and carbonates. The Regência Formation (Asmus et al., 1971) includes a relatively thick carbonate sequence comprising limestones, carbonate mudstones, and wackestones, with ostracods, gastropods and pelecypods fragments deposited in distal parts of the Espírito Santo Basin (Mohriak, 2003; França et al., 2007). The Albian carbonate platform is overlain by shales of Turonian to Palaeocene age (Unit S5), indicating a relative deepening of the basin (Gamboa et al., 2010; Gamboa et al., 2011; Ojeda, 1982, Demercian et al., 1993) (Fig. 2).

A mid-Eocene sequence boundary occurs across the entire southeast Brazilian margin and separates the early from the late drift stages (Gamboa et al., 2011) (Fig. 2). Above this boundary, Eocene to Holocene siliciclastic units (Units S6, S7 and S8; Fig. 2) were deposited during a regressive period recording sediment progradation on the continental slope (Demercian et al., 1993, Chang et al., 1992). At this time, clastic sediments filling the basin were derived from the erosion of coastal mountain ranges and from relatively local volcanic activity on the Abrolhos Plateau (Chang et al., 1992, Gamboa et al., 2010). Tuffs, volcanic breccias and hyaloclastites formed the bulk of the volcanoclastic input, whereas fine to coarse massive sandstones, conglomerates and siltstones were eroded from nearby mountains (Gamboa et al., 2010). Sediment transport occurred on Brazil's eastern margin in both drift stages, but was particularly important in the Late Oligocene to Holocene, as shown by the generation of vast channel systems (Viana et al., 2003, Fiduk et al., 2004; Alves, 2010). Between the Early/Mid Eocene and the Holocene, mass-transport deposits (MTDs) were also deposited in response to the uplift of coastal mountain ranges, subsequent tilting of the continental slope and halokinesis (Mohriak et al., 2008; Alves and Cartwright, 2010).

The seismic dataset used in this study was acquired on the upper (extensional) continental slope of the Espírito Santo Basin, offshore southeast Brazil (Fig 1a). Deformation in this region was greatly influenced by gravity-driven salt tectonics (Demercian et al., 1993; Davison, 1999, 2007; Gibbs et al., 2003; Fiduk et al., 2004; Alves, 2012), and is expressed in the form of complex structures such as salt rollers, vertical salt diapirs, seaward- and landward-dipping listric (roller) faults, normal faults, rollover anticlines and tectonic rafts (Figs. 3 and 4).

3. Dataset and methods

3.1. Dataset

The seismic block (BES-100) investigated in this study covers an area of 2,450 km^2 of the Espírito Santo Basin, in water depths ranging between 700 m and 1,970 m (Fig. 1). It was acquired using dual airguns and an array of 6 x 5,700 m long streamers. Data were recorded with a 2 ms vertical sampling interval, and a 12.5 x 12.5 m bin spacing. This configuration gives 57-fold coverage and a maximum lateral resolution of 12.5 m.

The seismic dataset was zero-phase migrated using a 3D Stolt pre-stack time migration algorithm. It displays a normal positive polarity so that an increase in acoustic impedance is represented by a peak and is red on the seismic sections. The vertical scale of the seismic dataset is two-way travel time (TWTT) and, for this study, it was limited to a recording length of about 5.0 s (Fig. 2). Velocity

information obtained from Alves (2012) was used in the depth conversions in this paper (Fig. 2). Based on a velocity range of 1900 to 2700 m/s, and the dominant frequency content of the seismic dataset (40 Hz), vertical seismic resolution ranges between 12 m in shallow Cenozoic strata and 17 m at Cretaceous level. Stratigraphic information from França et al. (2007) and Alves (2012) was used to identify, date and correlate the interpreted seismic horizons across the study area (Fig. 2).

3.2. Methods

Horizons and faults were mapped using Schlumberger's Petrel®. Prior to its mapping, the entire seismic volume was visually scanned and inspected to assess data quality and develop a quick understanding of main structural features in the study area, e.g. main relationships between sedimentary units and structures. The overall quality of the seismic dataset is good. However, some of the reflections are weak and chaotic within Cretaceous strata (Unit S4) (Figs. 3 and 4). As a result, we mapped eight age-constrained seismic units and correlated them with stratigraphic data in França et al. (2007) (Fig. 2). For the purposes of this study, we grouped the interpreted seismic units into two main seismic-stratigraphic packages: Cretaceous and Cenozoic (Fig. 2). The Cretaceous strata is crossed by seismic horizons H1 to H5, which span from the Aptian (118.5 Ma) to the Maastrichtian (67.2 Ma). Cenozoic strata is sub-divided by seismic horizons H6, H7 and the sea floor, spanning the Paleocene (67.5 Ma) to the Holocene (Fig. 2).

Distinct normal faults, including roller (listric), rollover, reactivated, radial and concentric faults, were imaged on TWTT structural maps (Figs. 5 and 8). A major advantage of the study area is that well-dated Late Cretaceous to Miocene unconformities truncate the interpreted fault families, thus allowing to relatively date the periods of fault movement below and above these unconformities (Fig. 13). The growth histories of these fault families were investigated by measuring their throws at regular intervals of 25 m along the strike of faults, except for large listric faults, which were measured at 125 m intervals. This complied with the minimum sampling interval of Tao and Alves (2019). The length of the interpreted faults ranges from 120-12,522 m, with maximum fault throws of 58-530 m (Table 1). The measured throw values were plotted against depth, to assess the vertical and lateral growth histories of faults in the study area (Figs. 9, 10, 11 and 12).

The throw-depth (T-Z) plots were analysed to determine whether a fault is blind or comprises a growth fault, and if it had been reactivated (Walsh and Watterson, 1989; Mansfield and Cartwright, 1996; Cartwright and Mansfield, 1998; Baudon and Cartwright, 2008). A reactivated fault is considered to have a stepped vertical throw profile. If there is a throw minimum and a negative gradient across a stratigraphic unconformity that has been offset by a fault, fault propagation is a result of "dip linkage" (Mansfield and Cartwright, 1996). If the throw has a stepped profile, but maintains a positive gradient, the fault is believed to have developed predominantly by "upward propagation" (Baudon and Cartwright, 2008).

Uncertainties associated with the measurement of fault-throw values may arise from the vertical sampling rate. The sampling interval, rather than the vertical stratigraphic resolution, determines accuracy when matching two correlative seismic reflection peaks or troughs (Baudon and Cartwright, 2008). An uncertainty in the positions of stratal terminations does introduce minimal error, associated with the position in depth of the recorded displacements. This is a function of the frequency content of the seismic dataset (Mansfield and Cartwright, 1996). Error associated with velocity estimate might also affect the throw values when converted to meters. Vertical sampling for the interpreted seismic volume is 2 ms.

4. Interpreted seismic units

Eight seismic units bounded by Late Cretaceous to Pliocene unconformities were mapped and correlated with stratigraphic data from França et al. (2007) and Alves (2012) (Fig. 2). The interpreted seismic units are grouped into two main stratigraphic seismic units, Cretaceous and Cenozoic (Fig. 2).

4.1. Cretaceous seismic units

The Cretaceous seismic units were named Units S1 to S5, and range from Aptian to Maastrichtian in age (Fig. 2).

4.1.1. Unit S1 (Early Aptian to Middle/Late Aptian)

Unit S1 comprises the syn-rift III sequence and the early post-rift sequence (Fig. 2). The unit is bounded by the Alagoas unconformity at its base and by evaporites (Unit S2) at its top (Fig. 2). Unit S1 belongs to the upper Nativo Group (Mariricu Formation) and comprises conglomerates, sandstones and shales deposited in lacustrine and sabkha environments (França et al., 2007). The unit comprises moderate to high amplitude, low frequency reflections (Fig. 2).

4.1.2. Unit S2 (Middle/Late Aptian to Early Albian)

Unit S2 comprises main salt structures (e.g., salt rollers, pillows and diapirs) in the study area (Figs. 3 and 4). The lower boundary of the unit (top of early post-rift sequence; Unit S1) consists of an irregular reflection of moderate to high amplitude. Its upper boundary coincides with the first continuous high-amplitude strata (carbonate platform; Unit S3) covering Unit S2 (Figs. 3 and 4). In the study area, Unit S2 forms triangular salt rollers and vertical diapirs (Figs. 3 and 4).

4.1.3. Unit S3 (Early Albian to Cenomanian)

Unit S3 comprises high-amplitude, low-frequency seismic reflections and was deposited above evaporites in Unit S2 (Figs. 3 and 4). The top of the unit is an angular unconformity in the proximal regions of the Espírito Santo Basin, changing laterally into a paraconformity in deeper waters (França et al., 2007). In the study area, Unit S3 is fragmented into discrete tectonic rafts (Figs. 3 and 4).

Unit S3 is part of the Barra Nova Group, which includes the São Mateus and Regência Formations, with sicliclastic and carbonate rocks deposited from the Albian to the Cenomanian on a shallow shelf (França et al., 2007). The São Mateus Formation consists of sandstones deposited in a proximal marine setting over a succession of shales, siltstones, and carbonates (França et al., 2007). The Regência Formation includes a relatively thick carbonate sequence comprising limestones, carbonate mudstones, and wackestones with ostracods, gastropods and pelecypods fragments deposited in distal parts of the Espírito Santo Basin (Asmus et al., 1971). The Barra Nova Group is bounded at its top by the Pre-Urucutuca unconformity (França et al., 2007) (Fig. 2).

4.1.4. Unit S4 (Cenomanian to Santonian)

Unit S4 comprises continuous, low-amplitude reflections (Figs. 3 and 4). The unit is locally deformed by closely spaced normal faults (Figs. 3 and 4). The lower boundary of the unit is sharp, and marked by growth onto major regional and counter-regional roller faults above Horizons 2 and 3 (Fig. 4). The upper boundary of the unit (H4) is an irregular high-amplitude reflection representing an unconformity of Santonian age (França et al., 2007).

Unit S4 is part of the lower Espírito Santo Group and Urucutuca Formation, comprising shales interbedded with conglomerates, limestones, and sandstones deformed from the Cenomanian to the Coniacian due to halokinesis (França et al., 2007). On the distal margin, dark shales and sands have been described by Cainelli and Mohriak (1999) and França et al. (2007).

4.1.5. Unit S5 (Late Santonian to Maastrichtian)

Unit S5 comprises low-moderate amplitude strata above Unit S4. The lower boundary of the unit is marked by an unconformity related to the incision of a Late Cretaceous channel system (horizon H4 - Golfinho Field; Vieira et al., 2007; Alves, 2012) (Fig. 5). This same boundary (H4) is marked by the appearance of high-amplitude reflections above a faulted succession that shows growth of strata onto roller faults (Fig. 4). A regional unconformity of Late Maastrichtian age marks the upper boundary of the unit (Vieira et al., 2007).

Unit S5 comprises the middle portion of the Urucutuca Formation (Fiduk et al., 2004; França et al., 2007) (Fig. 2). During the Coniacian-Maastrichtian, the Urucutuca Formation recorded the deposition of sandy turbidites sourced by the Fazenda Cedro and Regência palaeocanyons (França et al., 2007), leading to the accumulation of turbidites at its base and predominantly shales and sandstones in proximal parts of the basin (França et al., 2007). Unit S5 correlates with the topmost Cretaceous strata mapped in the study area (Fig. 2).

4.2. Cenozoic seismic units

The Cenozoic seismic units comprise the S6 to S8 units, which span the Paleocene to Holocene (Fig. 2).

4.2.1. Unit S6 (Paleocene to Early Eocene)

Unit S6 is shown as a unit with high-amplitude reflections that are locally deformed by closely spaced normal faults (Figs. 3 and 4). Its lower boundary coincides with an unconformity of Maastrichtian age (H5; Fig. 2). The upper surface of the unit is marked by another regional unconformity above which moderately faulted high-amplitude strata were deposited (H6). In Unit S6, the volcaniclastic Abrolhos Formation is interbedded with thick turbidites forming channelised bodies whose distribution was controlled by halokinesis (Cainelli and Mohriak, 1999; França et al., 2007; Mohriak, 2003).

4.2.2. Unit S7 (Eocene to Early Miocene)

Unit S7 is composed of prograding high-amplitude reflections (Figs. 2 and 4). Moreira and Carminatti (2004) relate this unit to successive regressive and transgressive events affecting the Brazilian margin. Unit S7 comprises turbidite sands intercalated with volcaniclastic deposits (França et al., 2007).

4.2.3. Unit S8 (Early Miocene to Holocene)

Unit S8 overlies Unit S7 in a concordant manner and is bounded at its top by the sea floor (Fig. 3). It consists of a package of high frequency, continuous and moderate to high-amplitude reflections (Fig. 2). The overall thickness of Unit S8 changes significantly where erosion occurred due to the development of channel complex systems.

Unit 8 correlates with the Rio Doce, Caravelas and the upper Urucutuca Formations (França et al., 2007). Strata in this unit comprise sandstones (Rio Doce Formation), calcarenites (Caravelas member) and turbidite sands and marls (Urucutuca Formation) (França et al., 2007). Thus, where Unit S8 is eroded by submarine channels, mass-transport complexes and channel-fill deposits predominate in Mid-Miocene and younger strata (França et al., 2007).

5. Rollover anticlines and associated structures

Seismic imaging shows that the study area is characterised by wide rollover anticlines developed above tectonic rafts, tectonic rafts separated by large listric (roller) faults and associated minibasins, rollover faults over wide rollover anticlines, salt rollers in the footwall of listric (roller) faults, reactivated pop-up structures and drag folds (Fig. 4). Tectonic rafts (Unit S3) form the core of broad rollover anticlines and commonly lie between or above salt rollers (Figs. 3 and 4). Where extension has been greatest and salt (Unit 2) completely evacuated, tectonic rafts lie directly on pre-salt units (Unit S1) (Fiduk et al., 2004; Alves, 2012) (Fig. 4).

It is clear in the seismic sections (Figs. 3 and 4) that the downthrown blocks associated with listric (roller) faults exhibit a larger component of vertical slip adjacent to the fault plane than it does at some distance from the fault plane, so that a rollover anticline develops. These rollover structures are of interest to the hydrocarbon industry as they may provide potential structural traps for hydrocarbon. The rollover geometry is the inevitable result of movement on a listric (roller) fault (Hamblin, 1965). Movement on such a curved fault plane

will tend to generate a 'gap' between the hanging-wall and footwall blocks (Fig. 14 a, b) which will be accomodated by the extensional collapse of the hanging-wall in either a ductile or brittle manner (Fig. 14 c, d). More frequently, deformation occurs as a result of a combination of both modes of deformation (brittle and ductile) to form a rollover anticline and associated fault structures (Fig. 14). In the study area, rollover anticlines trend in the N-S direction, sub-parallel to the strike of tectonic rafts (Figs. 5 and 6).

Moving into the basin (eastwards), salt rollers developed into a vertical salt diapir province (Fig. 3). Diapirs commonly form in relative deep water, where the rift basin had subsided more and correspondingly thicker autochthonous salt was deposited (Fiduk et al., 2004). Depending on their salt budget, some diapirs have ceased movement in the Cretaceous (Fiduk et al., 2004), while others are still growing near the modern sea floor (Fig. 3). The presence of withdrawal synclines adjacent to the salt diapir, and folded strata overlapping this diapir near the sea floor, suggest that the salt diapir is actively growing at present (Fig. 3). Radial faults are localised and distributed around the salt diapir and intersect both roller and rollover faults (Fig. 5). The TWTT structural maps in Fig. 8 highlight the geometry of rollover anticlines and their associated faults.

5.1. Roller (listric) faults

Roller (listric) faults comprise large regional (basinward-dipping) and counter-regional (landward-dipping) growth faults bounding tectonic rafts and minibasins (Fig. 4). These faults sole out at salt level (Unit S2) and the syn-rift III (Unit S1), in the places where the salt unit was almost completely removed (Fig. 4). Triangular salt rollers are observed towards the footwalls of these faults (Fig. 4). Some of the roller faults propagated vertically into Mid Paleogene strata (Unit S7) and terminate at the base of mass-transport deposits (H7), with no faults extending near the sea floor (Figs. 3 and 4). These faults accommodated gravity gliding of the overburden units along the basal salt (Unit S2) generating, at the same time, significant subsidence in adjacent salt minibasins (Fig. 4). In their immediate hanging-wall, salt minibasins show significant subsidence and denote the formation of drag folds, reactivated local pop-up structures and wider rollover anticlines (Fig. 4). The roller faults are less than 15 km-long (average 8.56 km), with a maximum throw of 530 m (average throw 470 m) (Table 1).

5.2. Rollover faults

Rollover faults comprise closely spaced sets of normal faults that are localised on top of the Cretaceous rollover anticlines (Figs. 3 and 4). These faults resulted from outer-arc stretching of strata overlying anticlinal structures. The faults dip in both basinward and landward directions, offsetting the Cretaceous Unit S4 (Figs. 3 and 4). In the study area, a significant part of rollover faults overlie tectonic rafts at depth (Alves, 2012). The progressive bending of rollover anticlines developed above rafts led to the progressive faulting of the Cretaceous Unit S4 by rollover faults (Figs. 3 and 4). These rollover faults accommodate a significant part of the bending strain affecting hanging-wall blocks of large roller faults, and areas recording post-salt extension of the supra-salt overburden.

5.3. Reactivated faults

Reactivated faults comprise densely spaced normal faults that are dominantly localised in the Paleogene strata (Unit S6) (Figs. 3 and 4), with some faults propagating into Late Cretaceous strata. Reactivated faults were initially formed by arching of the Late Cretaceous overburden above tectonic rafts, but were later deformed into local pop-up structures (Fig. 4). These faults were essentially rollover faults that suffered significant compression during the Late Cretaceous and Earliest Paleogene (Alves, 2012).

5.4. Concentric faults

Concentric faults are localised above extensional minibasins, i.e. in the space created by tectonic rafts. These faults occur within

extensional minibasins bounded by roller faults and are concentrically arranged, dipping towards the centre of such minibasins (Figs. 5 and 8). Concentric faults accommodate local strain on the tips of the oval-shaped salt minibasins formed on the hanging-wall blocks of roller faults during the main periods of raft-related extension. These faults are less than 5 km long (average 2,650 km), with a maximum throw of 55 m (average throw 50 m) (Table 1).

6. Fault geometries over rollover anticlines

The seismic sections in Figs. 3 and 4 highlight some of the features of faults formed above rollover anticlines. Above horizon H7, seismic reflections are chaotic and not affected by faults. Between H6 and H5 (Unit S6), the seismic expression of strata is markedly different in that seismic reflections are affected by closely spaced normal faults. Seismic reflections between H5 and H4 (Unit S5) are sparsely affected by faulting. Between H4 and H3 (Unit S4), the seismic expression of strata is again distinct from the units immediately above in that seismic reflections are highly disrupted and affected by closely spaced normal faults. Thus, three distinct tiers of faults can be recognised above rollover anticlines (Figs. 3 and 4).

6.1. Tier 1 Faults

Tier 1 faults comprise closely spaced normal faults that offset horizon H4 (Figs. 3 and 4). Throws die out downward towards the top of tectonic rafts, which are apparently unfaulted and flat-topped due to Santonian incision (Vieira et al., 2007). These faults have a maximum throw of 58 m, an average spacing of 250 m and trace lengths of 220-620 m (Table. 1). Tier 1 faults are located on top of the Late Cretaceous rollover anticlines (Unit S4), and are thus interpreted as rollover faults (Figs. 3 and 4). These faults are aligned concentrically in front of listric (roller) faults, generating large half-moon structures and a curved-polygonal fault pattern over rollover anticlines (Figs. 7a and 8a). Tier 1 faults are dated as Cenomanian to Campanian (Figs. 2 and 13).

6.2. Tier 2 Faults

Tier 2 faults comprise sparsely spaced normal faults that offset horizon H5 (Figs. 3 and 4). Throws die out downwards towards horizon H4, which is highly faulted, and also upward into Unit S6. These faults appears to overlap and link with other faults offsetting horizons H4 and H6 (Fig. 4). Tier 2 faults have a maximum throw of 55 m, an average spacing of 310 m and trace lengths of 280-650 m (Table. 1). These faults are localised on top of the Late Cretaceous rollover anticlines (Unit S5), and are characterised by a large range of strikes, rarely showing an equal distribution of fault strikes. As a result, they form a rectangular-polygonal pattern over rollover anticlines (Figs. 7b and 8b). Tier 2 faults accommodate some part of the bending strain occurring in the hanging wall block of large roller faults. These faults were essentially rollover faults that suffered significant compression in the Late Cretaceous. Tier 2 faults are dated as Late Santonian to Maastrichtian (Figs. 2 and 13).

6.3. Tier 3 Faults

It is clear in the seismic sections (Figs. 3 and 4) that a number of densely spaced normal faults offset Unit S6. Throws die out downwards in Unit S6 and below horizon H5. Their upper tips terminate in Unit S6 and above horizon H6 (Figs. 3 and 4). Thus, these faults were classified as Tier 3 faults. Tier 3 faults dominantly offset the Paleogene strata (Unit S6), with some faults propagating and linking with Tiers 1 and 2 faults (Fig. 4). These faults have a maximum throw of 50 m, an average spacing of 210 m and trace lengths of 120-550 m (Table. 1). Tier 3 faults are characterised by a diverse range of strikes, and rarely show equal distribution of fault strike orientations - thus forming an irregular-polygonal pattern over rollover anticlines (Figs. 7c and 8c). Tier 3 faults are dated as Paleocene to Eocene (Figs. 2 and 13).

In general, the geometry of polygonal faults resembles the polygonal networks of cracks and fractures that occur at a variety of

scales in natural media in response to volume changes, e.g. cracks in ceramic glasses and concrete, desiccation cracks in muds and playa lakes, ice-wedge polygons in frozen ground and columnar joints in lavas (Allen, 1987; Korvin, 1992). In the study area, the observed fault patterns are not entirely polygonal because not all the faults connect to create closed cells in plan view. Some of the maps we compiled reveal fault patterns that resemble the incomplete stage of desiccation in muds, in which not all the cracks have connected to make closed polygons (Plummer and Gostin, 1981; Allen, 1987) (Figs. 7 and 8). However `polygonal' still seems to be the best approximation of the faults' plan view geometry as planar, curved and sinuous fault traces are distributed in a wide variety of orientations and connect to form both closed and open multi-sided cells (Lonergan et al., 1998).

A variety of fault geometries have been identified off Espírito Santo based on fault trace orientation, intersection angle, spacing, and fault trace linkage or connectivity (Figs. 7 and 8). These fault geometries include: 1) curved polygonal patterns dominated by curved fault traces with a broad spread of intersection angles, between 90^0 and 140^0 (Figs. 7a and 8a) (Lonergan et al., 1998); 2) regular-rectangular polygonal patterns where the majority of intersection angles are orthogonal (Figs. 7b and 8b), and 3) irregular, poorly-connected fault patterns with short fault traces, which tend to be grouped or aligned in clusters (Figs. 7c and 8c). In the published literature, such geometries have been attributed to four genetic mechanisms: gravity collapse, density inversion, syneresis and compactional loading (Cartwright et al. 2003).

Curved (Figs. 7a and 8a) and regular-near-rectangular (Figs. 7b and 8b) patterns can be considered to be two end-member geometries, with the irregular pattern representing an intermediate form (Figs. 7c and 8c). This suggests that connectivity may be a property that reflects the `maturity' of the fault network, with low connectivity patterns forming where the faults have not continued to grow and later link-up to form a highly connected network (Lonergan et al., 1998). In some cases, the lack of connectivity may only be apparent and occur as a function of the fault dimension, data resolution and quality (Tao and Alves, 2019). If the faults are smaller and more closely spaced, forming at a scale close to the data resolution then only the larger faults will be imaged, and the smaller connecting fault segments will remain unresolved in seismic data (Lonergan et al., 1998; Tao and Alves, 2019).

7. Mode of fault reactivation

Fault reactivation has been described as resulting from further propagation of pre-existing faults after a significant period of dormancy (e.g. Cartwright et al., 1995; Baudon and Cartwright, 2008). The growth history for the interpreted faults in the Espírito Santo Basin was investigated using vertical throw-depth (T-Z) plots (Figs. 9, 10 and 11). These faults were grouped into two main categories based on their mode of reactivation, as revealed by the throw-depth plots. These groups are: 1) reactivation by segment linkage, and 2) reactivation by upward propagation. Faults reactivated by segment linkage show throw profiles with zones of throw maxima separated from pre-existing faults by a region with throw minima and steepening throw gradients (Figs. 9, 10 and 11). Faults reactivated by upward propagation present throw-depth plots that maintain a vertical, positively stepped gradients (Baudon and Cartwright, 2008) (Fig. 12).

7.1. Reactivation by segment linkage.

The throw-depth (T-Z) plots in Tier 1, 2 and 3 faults show a typical mode of reactivation by segment linkage (Figs. 9, 10 and 11). This mode of reactivation is recognised by zones of throw maxima separated from pre-existing faults by areas with throw minima and steepening of the throw gradients (Figs. 9, 10 and 11). The throw profiles of these faults do not always have single positive gradients, and are characterised by throw profiles resembling C-type or M-type patterns between the upper-tip point and immediate throw minima (Baudon and Cartwright, 2008) (Figs. 9a, 10a and 11a). The presence of alternating zones of pre-

existing throw maxima and minima in the throw distribution contour also point out to faults reactivating via the linkage of individual segments (Figs. 9b, 10b and 11b).

7.1.1. Fault reactivation in Tier 1

Tier 1 faults are localised and restricted to the top Cretaceous rollover anticlines, i.e. Unit S4 (Figs. 3 and 4). The throw-depth plots of these faults show truncation at horizon H4, terminating downwards within Unit S4; they never cross-cut horizon H3 (Fig. 9a). The vertical throw-depth plots of these faults resemble a C-type pattern between the upper-tip point and immediate throw minima (Fig. 9a). The lack of near-zero throw values at horizon H4 confirms erosion of the fault tips by Late Santonian to Maastrichtian channel systems (Fig. 9a).

The mode of reactivation in Tier 1 faults is illustrated with reference to the throw distribution plots in Fig. 9. Segments A, B and C are pre-existing fault segments with throw maxima. Each fault segment coalesces with other segments that are similar in dip and strike directions to form a larger fault (Fig. 9). Segment A propagates and links with Segment C (plots 1, 2, 4 and 5; Figs. 9a). In a similar fashion, Segment B was reactivated to link with Segments A and C (plot 3; Figs. 9a). Segment C is truncated upwards at horizon H4. This fault segment appears to be eroded by the incision of Late Santonian to Maastrichtian channel systems (Vieira et al., 2007). Thus, the throw-depth plots of these faults reveal fault segment linkage as multiple peaks of throw maxima separated by throw minima (Fig. 9a).

Throw distribution contours provide additional information regarding segment linkage in Tier 1 faults (Fig. 9b). Segments with throw maxima A, B and C are pre-existing fault segments that were initiated at different depths. Each segment is separated from each other by a zone of throw minima and steepening of throw gradients as expected for faults reactivating by segment linkage (Fig. 9b). Similarly, the throw-distance (T-X) plots in Fig. 9c suggest modes of reactivation by segment linkage. The throw-distance plots have two segments of throw maxima A and C separated by a throw minima, as expected when growing faults by segment linkage. In other words, Segment A was reactivated and linked with Segment C (Fig. 9c).

7.1.2. Fault reactivation in Tier 2

Tier 2 faults typically offset Late Cretaceous strata (Unit S5). Some of these faults appears to overlap and link with faults from Tiers 1 and 3 (Fig. 4). The throw-depth plots of these faults tip out upwards just above horizon H6, and downwards into Unit S4 (Fig. 10a). Their vertical throw profiles are characterised by M-type and or C-type patterns between the upper-tip point and immediate throw minima (Fig 10a).

The throw-depth plots of Tier 2 faults indicate a mode of reactivation dominated by segment linkage (Fig. 10). Along horizon H4 there is a throw maxima leading to decrease in throw at horizon H5, followed by a further increase in throw upwards (Fig. 10a). This character reflects reactivation by segment linkage, where two separate faults have propagated towards each other. Multiple throw peaks on throw-depth plots show that fault segment linkage is a common process (Figs. 10a and 10b). Towards the south, Segment A was reactivated to link with Segment B (plots 1, 2 and 3; Fig. 10a and plot 1; Fig. 10b). Further north, Segment B switches and links with Segment C (plots 4 and 5; Fig. 10a and plot 2; Fig. 10c). Segment B terminates upwards just above horizon H6 (Fig. 10a). The similarity between the dips and strikes of these fault segments, nucleating at different depths, points out to one of the key characteristics of faults reactivation by segment linkage.

7.1.3. Fault reactivation in Tier 3

Tier 3 faults are dominantly localised within Paleogene strata (Unit S6) (Fig. 4). These faults tip out upwards just above horizon H6, and downwards just below horizon H5. Thus, their throw profiles resemble M-type patterns (Fig. 11a). Tier 3 faults show a mode of reactivation by segment linkage (Fig. 11).

Segments A, B, C and D are pre-existing fault segments with throw maxima (Fig. 11). Each segment is separated by a throw minima, as expected for reactivation by segment linkage (Fig. 11). Towards the south, Segment A is reactivated by dip linkage with Segment C (plot 1; Figs. 11a). Further north, Segment A switches and links with Segment D (plots 4 and 5; Fig. 11a). Segment B was reactivated to link with Segments A and C (plot 2; Fig. 11a). These sharp changes in throw values are interpreted to be a consequence of reactivation by segment linkage of individual fault segments. Moreover, the throw-distance plots in Fig 11c indicate a mode of reactivation by segment linkage; they show multiple peaks of throw maxima separated by a sharp change in throw gradients (Fig. 11c).

7.2. Reactivation by upward fault propagation

Large listric (roller) faults that bound the distinct fault tiers and wide rollover anticlines exhibit a typical vertical, positive stepped throw gradients (Fig. 12). These faults show major breaks in throw gradients around horizons H4 and H5, i.e. the Campanian and Paleocene unconformities (Fig 12a, c). Throw-depth plots for these faults can be divided into three parts; lower, central and upper parts. The lower part contains Unit S4, and shows throw maxima between 400 m and 530 m (Fig. 12a, c). The central part contains Unit S5 and reveals an abrupt step in throw profiles, with throws between 150 m and 300 m (Fig. 12a, c). The upper part contains Unit S6 and shows almost constant positive throw gradients with no significant variations. It records fault throws throws between 2 m and 120 m (Fig. 12a, c).

The decrease and vertical positive step in throw gradients recorded by the roller faults can be related to the effects of reactivation by upward propagation from parent faults above a detachment surface (Unit S2) (e.g. Baudon and Cartwright, 2008). Also, the absence of alternating zones of pre-existing throw maxima (and minima) in throw contour maps, and the observed uniform lateral continuity in throw gradients, relate to reactivation of roller faults by upward propagation (Fig. 12b, d).

8. Discussion

8.1. Tiered faulting vs. distinct tectonic episodes of gravitational gliding

The continental margin of southeast Brazil is primarily associated with the continental break-up of Gondwana in the Late Jurassic to Early Cretaceous, and subsequent opening of the South Atlantic Ocean (Chang et al., 1992; Davison, 1999; Meisling et al., 2001). After rifting ceased, gravity tectonics became the primary deformational process in the Espírito Santo Basin, triggered by differential sediment loading, gravitational spreading and gliding of the supra-salt overburden. Uplift and tilting of the continental margin has been an intermittent, but important factor impacting these latter phenomena (Demercian et al., 1993; Alves et al., 2009; Fiduk et al., 2004).

On the continental slope of southeast Brazil, gravitational gliding induced a continuum of deformation and contributed significantly to shaping the supra-salt overburden - as expressed by complex structures such as listric (roller) faults, wide rollover anticlines, closely spaced collapsed growth fault crests, reactivated faults and folds, salt rollers and tectonic rafts (Figs. 3 and 4). Three distinct Late Cretaceous to Paleogene tectonic stages of gravitational gliding are recognised in the study area; initial, renewed and late stages of gravitational gliding (Fig. 15).

The initial stage (post-Albian to Coniacian) caused the post-salt strata (Unit S3) to be fragmented into discrete blocks of strata or rafts separated by large listric (roller) faults and associated minibasins (Fig. 15a). This stage is characterised by downslope movement of rafts, the development of large listric (roller) faults controlling seafloor topography during extension, significant subsidence in half-grabens adjacent to roller faults, development of rollover anticlines above rafts, and initiation of normal faults on top of rollover anticlines to accommodate the buckling of the post-raft overburden. (Figs. 14 and 15a).

The renewed stage (Early Santonian to Early Paleogene) caused the rafts (Unit S3) to be translated downslope until salt welds were formed, i.e. rafts became grounded over pre-salt units. The grounding (welding) of rafts over the pre-salt strata was progressive, and accompanied by moderate translation of blocks during the Early Paleogene (Alves, 2012) (Fig.15b). This stage is characterised by discrete blocks of strata (rafts), seaward- and landward-dipping listric (roller) faults, wide rollover anticlines, rollover faults, reactivated faults, salt rollers and growth strata infilling minibasins (Figs. 14c and 15b).

The late stage of gravitational gliding (Mid Paleogene to Holocene) caused the diachronous grounding of rafts, thus promoting significant fault reactivation and stratal shortening in the Late Cretaceous to Paleogene strata (Fig. 15c). This stage is characterised by large blocks of grounded strata (rafts), wide rollover anticlines whose axes are sub parallel to the strike of rafts, seaward- and landward-dipping listric (roller) faults, normal faulting over rollover anticlines, fault reactivating, reactivated pop up structures, drag folds, salt rollers, salt diapir and growth strata infilling minibasins (Figs. 3, 4, 14d and 15c).

8.2. Impact of the gravitational gliding of tectonic rafts on fault geometry

The Late Cretaceous to Paleogene gravitational gliding of tectonic rafts induced a continuum of post-salt overburden deformation that controlled fault geometry over rollover anticlines, generating three distinct tiers (Figs. 4, 7, 8 and 13). Each fault tier has distinct fault spacings, geometries, fault trace shapes and fault strikes orientations (Figs. 4, 7 and 8). These fault tiers include; Tiers 1, 2 and 3. Each fault tier geometry is associated with distinct tectonic episodes of gravitational gliding (Fig. 15).

Tier 1 faults (Cenomanian to Campanian) comprise closely spaced normal faults that resulted from the outer-arc stretching of the Late Cretaceous strata (Unit S4) overlaying tectonic rafts (Unit S3). These faults accommodate a significant part of the bending strain occurring in the hanging-wall blocks of listric (roller) faults during the initial tectonic stage of gravitational gliding (Fig. 15a). The faults are aligned concentrically in front of listric (roller) faults, generating large half-moon structures and curved-polygonal fault patterns over rollover anticlines (Figs. 7a and 8a). A significant part of these faults overlie tectonic rafts offshore Espírito Santo (Alves, 2012).

Tier 2 faults (Late Santonian to Maastrichtian) comprise closely spaced normal faults with a diverse range of fault strikes that form a rectangular-polygonal pattern over rollover anticlines (Figs. 7b and 8b). The progressive bending of rollover anticlines above tectonic rafts during the renewed stage of gravitational gliding led to the progressive faulting of the overburden strata by these faults. Tier 2 faults accommodate some of the bending strain and post-salt extension in overburden strata during the renewed stage of gravitational gliding (Fig. 15b).

Tier 3 faults (Paleocene to Eocene) comprise densely spaced set of normal faults with a discrete range of fault strikes revealing an irregular-polygonal pattern over rollover anticlines (Figs. 7c and 8c). Differences in the timing of (diachronous) grounding of tectonic rafts are responsible for the development of these faults, as well as reactivated local pop-up structures and drag folds formed adjacently to roller faults (Fig. 4). Tier 3 faults are associated with the later tectonic stages of gravitational gliding in the Espírito Santo Basin (Fig. 15c). The geometric variations recognised in the distinct fault tiers, i.e. from curved to rectangular and then irregular polygonal patterns, reflect the effect of distinct episodes of gravitational gliding in the underlying tectonic rafts (Fig. 15).

8.3. Impact of the gravitational gliding of tectonic rafts on fault reactivation and growth

Fault reactivation has been described as the growth of pre-existing faults by further propagation after a significant period of quiescence (e.g. Cartwright et al., 1995; Baudon and Cartwright, 2008). Two distinct modes of

faults reactivation were identified in the study area: segment linkage and upward propagation. Both modes of fault reactivation are recognised by typical stepped profiles in throw gradients. Differences in the throw-distribution provide insights into the recognition of either mode (Figs. 9, 10, 11 and 12).

Tier 1, 2 and 3 faults were reactivated by segment linkage, i.e. by fault growth through coalescence of multiple fault segments. This mode of fault reactivation is recognised by a zone of throw maxima that is separated from the pre-existing parts by a zone of throw minima and steepening of the throw gradients (Figs. 9, 10, and 11). Their throw-depth plots do not always show single positive gradients, and are mostly characterised by throw profiles that resemble C-type or M-type patterns between the upper-tip point and immediate throw minima (Baudon and Cartwright, 2008). These distinct fault tiers are in line with the proposed coherent fault model (e.g. Cartwright et al., 1995) as their preferential mode of growth was in both the vertical and horizontal directions.

The listric (roller) faults that bound the distinct fault tiers were reactivated by upward propagation. This mode of reactivation is recognised by vertical positive steps in throw gradients (Fig. 12). The faults are characterised by breaks in throw gradients corresponding to horizons H4 and H5, i.e. the Campanian and Paleocene unconformities (França et al., 2007) (Fig 12a, c). These breaks in throw gradients are attributed to lithological changes during fault propagation through mechanical barriers. Contrasts in impedance above and below these boundaries are enough to cause this type of changes in throw gradients. The significant reduction in fault throws above horizon H4 is due to the presence of weak Turonian to Paleocene shales (Unit S5) above a high impedance (i.e. competent) carbonate platform (Unit S4) (Ojeda, 1982; França et al., 2007). Therefore abrupt decreases in throw, and the vertical positive steps in throw gradients recorded by the roller faults, can be attributed to be the effects of reactivation by upward propagation from parent faults above a detachment surface, or décollement (Baudon and Cartwright, 2008) (Fig. 12).

8.4. Tiered faulting vs. discrete tectonic episodes on the Southeast Brazilian margin

Early Cretaceous to Pliocene tectonic episodes, i.e. those related to the Andean Orogeny and the emplacement of the Abrolhos Plateau, caused episodic margin uplift and tilting, as reflected by the rise of coastal mountain ranges in the Santonian (Mégard, 1984; Mégard et al., 1984; Bueno, 2004; Fiduk et al., 2004). These discrete tectonic episodes, which include the Mochica (Late Albian), Peruvian (Late Cretaceous), the Incaic (Eocene) and Quenchua 1 (Early Miocene), Quenchua 2 (Upper Miocene), Quenchua 3 (Pliocene), as well as the emplacement of the Abrolhos Plateau in the Eocene, are the main events that influenced the regional stress regimes in southeast Brazil (Figs. 2 and 13) (Gregory-Wodzicki, 2000; Mégard, 1984; Lima, 1999; Cobbold et al., 2007). During specific tectonic episodes, sediment progradation was triggered by the uplift of coastal ranges, following the reactivation of segments of the Brazilian margin (Cobbold et al., 2010). Cobbold et al. (2010) argue that because post-rift inversion episodes are synchronous with phases of orogenesis in the Andes, a likely cause of inversion structures offshore Brazil is plate-wide horizontal compression.

In the study area, reactivated structures (pop-up anticlines, drag folds, reactivated faults; Figs. 4 and 13) formed between horizons H4 (Late Santonian) and H6 (Early Eocene), with the bulk of inversion occurring below horizon H6 (Eocene), i.e. prior to the Incaic tectonic phase (Figs. 2 and 13). These structures were controlled locally by prolonged overburden faulting, and by the continued movement of deeply buried rafts. In particular, local pop-up structures are, in the study area, invariably associated with laterally shortened anticlines formed upslope or above grounded rafts, or to the flip-flop reactivation of roller faults as thrusts by moving rafts (Alves, 2012) (Fig. 4). Thus, grounded rafts acted as hard and soft buttresses during renewed gravity gliding as the margin was uplifted and exhumed. In contrast, downslope moving rafts shortened inter-raft

extensional basins as pop-ups. In fact, intra-raft salt structures (rollers) were able to localise strain downdip from rafts, whilst grounded, or slower-moving, rafts acted as buttresses to focus shortening on their updip flanks.

Tectonic tilting and uplift of the margin, and subsequent downslope movement of tectonic rafts, is a possible regional trigger to the reactivation of earlier extensional features as inversion structures for the more recent tectonic phases, i.e. the Incaic (Eocene) and Quenchua 1 (Early Miocene), Quenchua 2 (Upper Miocene) and Quenchua 3 (Pliocene) phases (Demercian et al., 1993; Cobbold et al., 2001). However, tectonic reactivation of tectonic rafts offshore Espírito Santo (Late Cretaceous to Paleocene) clearly predates the Incaic (Eocene) and Quenchua (Neogene) phases (Figs. 2 and 13). Alves (2012) postulated that the principal phase of crustal shortening in Espírito Santo Basin reflects the early stages of Andean convergence, i.e. the Mochica (Late Albian) and Peruvian (Late Cretaceous) phases, but that fault and anticline reactivation can be significantly diachronous when considering distinct structures, and zones, of the Espírito Santo Basin.

9. Conclusions

The detailed mapping of stratigraphic horizons and faults, statistical analyses of fault displacement using high-quality 3D seismic reflection data from the proximal region of the Espírito Santo Basin, southeast Brazil provided us with important insights into the geometry and growth history of normal faults formed over rollover anticlines. These anticlines were reactivated during gravitational gliding of tectonic rafts. The main conclusions of this work are as follows:

1. In the proximal extensional parts of the Southeast Brazilian Margin, Late Cretaceous to Paleogene gravitational gliding of tectonic rafts, intermittent uplift and tilting of the continental slope during the Andean orogeny, and emplacement of the Abrolhos Plateau, induced a continuum of internal deformation that is expressed in the form of complex structures. These include listric (roller) faults, wide rollover anticlines, closely spaced collapsed growth fault crests, reactivated faults and folds, vertical salt diapirs, salt rollers and large blocks of strata (rafts).

2. The Late Cretaceous to Paleogene gravitational gliding of tectonic rafts induced a continuum of post-salt overburden deformation that organised normal faults over rollover anticlines into three distinct fault geometries; from curved to rectangular and later irregular polygonal fault patterns. These fault patterns are the result of distinct episodes of gravitational gliding offshore Espírito Santo, meaning that the curved, rectangular and irregular polygonal fault patterns are related to the initial, renewed and later stages of gravitational gliding, respectively. The cessation of the gravitational gliding of tectonic rafts depended on the complete grounding of rafts above pre-salt strata, or the gravitational stabilisation of rafts imposed by sediment loading and cessation of tectonic uplift (and tilting) of the continental slope.

3. The downslope translation and grounding (welding) of tectonic rafts on sub-salt strata controlled the degree of overburden deformation. Thus, enhanced fault reactivation relates to the degree of welding between sub- and supra-salt strata, which potentially promotes the migration of hydrocarbons from sub-salt source units into supra-salt reservoirs.

4. The rollover geometry over tectonic rafts is the inevitable result of the propagation of listric (roller) faults. Movement on such a curved fault plane will tend to generate a ‘gap’ between the hanging-wall and footwall, which will be accommodated by the collapse of the hanging-wall in either a ductile or brittle manner.

5. Distinct fault tiers over rollover anticlines were reactivated by segment linkage, i.e. fault growth through the coalescence of multiple fault segments. The roller (listric) faults that bound the rollover anticlines were reactivated by upward propagation from

parent faults above a detachment surface, i.e. the Aptian salt.

Acknowledgements

Petroleum Technology Development Fund (PTDF), Nigeria was greatly acknowledge and thanked for funding the first author Ph.D. research study, in which this research paper was derived. We acknowledge CGG-Veritas for the permission to use and publish seismic data for this research paper and Schlumberger for the provision of Petrel® software for seismic interpretation. The comments, suggestions and constructive reviews by the anonymous reviewers (Webster Mohriak and Chris Morley) and editor (Ian Alsop) greatly improved the scientific content of this manuscript.

References

Allen, J. R. (1987) Desiccation of mud in the temperate intertidal zone: studies from the Severn Estuary and eastern England. Philosophical Transactions of the Royal Society of London B. 315, 127-156.

Alves, T. M., Cartwright, J. A., 2010. The effect of mass-transport deposits on the younger slope morphology, offshore Brazil. Marine and Petroleum Geology, 27**,** 2027-2036.

Alves, T. M., 2010. 3D Seismic examples of differential compaction in mass-transport deposits and their effect on post-failure strata. Marine Geology, 271**,** 212-224.

Alves, T. M., 2012. Scale-relationships and geometry of normal faults reactivated during gravitational gliding of Albian rafts (Espírito Santo Basin, SE Brazil). Earth and Planetary Science Letters, 331**,** 80-96.

Alves, T. M., Cartwright, J., Davies, R. J., 2009. Faulting of salt-withdrawal basins during early halokinesis: effects on the Paleogene Rio Doce Canyon system (Espírito Santo Basin, Brazil). AAPG bulletin, 93**,** 617-652.

Anette, B.M.T., Rotevatn, A., Jackson, C.A.L., Fossen, H., Gawthorpe, R.L., 2013. Growth of normal faults in multilayer sequences: a 3D seismic case study from the Egersund Basin, Norwegian North Sea. Journal of Structural Geology, 55, 1–20.

Asmus, H.E., Gomes, J.B., Pereira, A.C.B., 1971. Integração geológica regional da bacia do Espírito Santo. Relatório Interno, PETROBRAS.

Barnett, J.A., Mortimer, J., Rippon, J.H., Walsh, J.J., Watterson, J., 1987. Displacement geometry in the volume containing a single normal fault. AAPG Bull. 71, 925-937.

Baudon, C., Cartwright, J., 2008. The kinematics of reactivation of normal faults using high resolution throw mapping. Journal of Structural Geology, 30**,** 1072-1084.
Barnett, J.A., Mortimer, J., Rippon, J.H., Walsh, J.J., Watterson, J., 1987. Displacement geometry in the volume containing a single normal fault. AAPG Bull. 71, 925-937.

Bruhn, C. H., Walker, R. G., 1997. Internal architecture and sedimentary evolution of coarse-Grained, turbidite channel-levee complexes, Early Eocene Regência Canyon, Espirito Santo Basin, Brazil. Sedimentology, 44**,** 17-46.

Brun, J.-P., Mauduit, T.P.O., 2009. Salt rollers: Structure and kinematics from analogue modelling. Marine and Petroleum Geology 26, 249-258.

Bueno, G.V., 2004. Event diachronism in the South Atlantic rift. Bol. Geociênc. Petrobras 14, 203–229.

Cainelli, C. and Mohriak, W.U., 1999. Some remarks on the evolution of sedimentary basins along the eastern Brazilian continental margin. Episodes, 22 (3), 206-216.

Cartwright, J. A., Trudgill, B. D., Mansfield, C. S. 1995. Fault growth by segment linkage: An explanation for scatter in maximum displacement and trace length data from the Canyonlands Grabens of SE Utah. Journal of Structural Geology, 17, 1319-1326.

Cartwright, J.A., Mansfield, C.S., 1998. Lateral displacement variation and lateral tip geometry of normal faults in the Canyonlands National Park, Utah. Journal of Structural. Geology. 20, 3–19.

Cartwright, J., Trudgill, B., Mansfield, C., 2000. Fault growth by segment linkage: An explanation for scatter in maximum displacement and trace length data from the Canyonlands grabens of SE Utah: Reply. Journal of Structural Geology 22, 141-143.

Cartwright, J., James, D., and Bolton, Al., 2003. The genesis of polygonal fault system: a review. Geological Society, London, Special Publications, 216, 223-243.

Chang, H. K., Kowsmann, R. O., Figueiredo, A. M. F., Bender, A., 1992. Tectonics and stratigraphy of the East Brazil Rift system: an overview. Tectonophysics, 213**,** 97-138.

Cobbold, P.R., Rossello, E.A., Roperch, P., Arriagada, C., Gómez, L.A., Lima, C., 2007. Distribution, timing, and causes of Andean deformation across South America. In: Ries, A.C., Butler, R.W.H., Graham, R.H. (Eds.), Deformation of the Continental Crust: The Legacy of Mike Coward: Geological Society, London, Special Publications, 272, pp. 321–343.

Cobbold, R.R., Chiossi, D., Green, P.F., Japsen, Bonow, J.M., 2010. Compressional reactivation of the Atlantic Margin of Brazil: structural styles and consequences for hydrocarbon exploration. AAPG International Conference and Exhibition. American Association of Petroleum Geologists, Rio de Janeiro, Brazil, #30114.

Cramez, C., Jackson, M.P.A., 2000. Superimposed deformation straddling the continental–Oceanic transition in deep-water Angola. Mar. Pet. Geol. 17, 1095–1109.

Davison, I., 2007. Geology and tectonics of the South Atlantic Brazilian salt basins. Geological Society, London, Special Publications, 272**,** 345-359.

Davison, I., 1999. Tectonics and hydrocarbon distribution along the Brazilian South Atlantic margin. Geological Society, London, Special Publications, 153**,** 133-151.

Dawers, N.H., Anders, M.H., 1995. Displacement-length scaling and fault linkage. Journal of Structural Geology. 17, 607–614.

Demercian, S., Szatmari, P., Cobbold, P. 1993. Style and pattern of salt diapirs due to thin-skinned gravitational gliding, Campos and Santos basins, offshore Brazil. Tectonophysics, 228**,** 393-433.

Duval, B., Cramez, C., Jackson, M.P.A., 1992. Raft tectonics in the Kwanza Basin, Angola. Marine and Petroleum Geology 9, 389-404.

Faulkner et al. (2010).

Fiduk, J. C., Brush, E. R., Anderson, L. E., Gibbs, P. B., Rowan, M. G., 2004. Salt deformation, magmatism, and hydrocarbon prospectivity in the Espirito Santo Basin, offshore Brazil. Salt-sediment interactions and hydrocarbon prospectivity: Concepts, applications, and case studies for the 21st century: Proceedings of Gulf Coast Section SEPM Foundation Bob F. Perkins Research Conference, 2004. SEPM, 370-392.

Fort, X., Brun, J., Chauvel, F., 2004. Salt tectonics on the Angolan margin, syn-sedimentary deformation processes. AAPG Bull. 88, 1523–1544.

França, R. L., Del Rey, A. C., Tagliari, C. V., Brandão, J. R., Fontanelli, P. D. R., 2007. Bacia do Espírito Santo. Boletim de Geociencias da PETROBRAS, 15**,** 501-509.

Gamboa, D., Alves, T., Cartwright, J., Terrinha, P., 2010. MTD distribution on a 'passive'continental margin: the Espírito Santo Basin (SE Brazil) during the Palaeogene. Marine and Petroleum Geology, 27**,** 1311-1324.

Gamboa, D., Alves, T., Cartwright, J. 2011. Distribution and characterization of failed (mega) blocks along salt ridges, southeast Brazil: Implications for vertical fluid flow on continental margins. Journal of Geophysical Research: Solid Earth (1978–2012), 116.

Gaullier, V., Brun, J.P., Gue´rin, G., Lecanu, H., 1993. Raft tectonics: the effects of residual topography below a salt de´collement. Tectonophysics 228, 363-381.

Gibbs, P. B., Brush, E. R., Fiduk, J. C., 2003. The evolution of the syn rift and transition phases of the central/southern Brazilian and W. African conjugate margins: the implications for source rock distribution in time and space, and their recognition on seismic data. 8th International Congress of the Brazilian Geophysical Society, September 14-18, 2003 Brazil.

Gregory-Wodzicki, K.M., 2010. Uplift history of the Central and Northern Andes: a review. Geol. Soc. Am. Bull. 112, 1091–1105.

Guardado, L.R., Gamboa, L.A.P. and Lucchesi, C.F., 1989. Petroleum geology of the Campos Basin. a model for a producing Atlantic-type basin. In: J.D. Edwards and P.A. Santogrossi (Editors), Divergent/Passive Margin Basins. Am. Assoc. Pet. Geol. Mem., 48: 3-79.

Hamblin, W.K., 1965. Origin of 'reverse drag' on the down-throw side of normal faults. Geological Society of American Bulleting. 76, 1145-1164.

Koleydone et al. (2003)

Korvin, G. 1992. Fractal models in the Earth Sciences. Elsevier Science Ltd, Oxford, Amsterdam, London.

Lima, C., 1999. Expressions topographiques et structurales de l'état de compression généralisée au sein de la plaque sud-américaine. PhD Thesis, Université de Rennes 1, France.

Lohr, T., Krawczyk, C.M., Oncken, O., Tanner, D.C., 2008. Evolution of a fault surface from 3D attribute analysis and displacement measurements. Journal of Structural Geology 30, 690-700.

Lonergan, L., Cartwright, J.A. & Jolly, R. 1998. 3-D Geometry of Polygonal Fault Systems. Journal of Structural Geology, 20, 529-548.

Mansfield, C.S., Cartwright, J.A., 1996. High resolution fault displacement mapping from three-dimensional seismic data: evidence for dip linkage during fault growth. Journal of Structural Geology. 18, 249–263.

Mansfield, C., Cartwright, J., 2001. Fault growth by linkage: observations and implications from analogue models. J. Struct. Geol. 23, 745–763.

Mauduit, T., Guerin, G., Brun, J.P., Lecanu, H., 1997. Raft tectonics: the effects of basal slope angle and sedimentation rate on progressive extension. Journal of Structural Geology 19, 1219-1230.

McLeod, A.E., Dawers, N.H., Underhill, J.R., 2000. The propagation and linkage of normal faults: insights from the Strathspey-Brent-Statfjord fault array, northern North Sea. Basin Res. 12, 263-284.

Mégard, F., 1984. The Andean orogenic period and its major structures in central and northern Peru. J. Geol. Soc. Lond. 141, 893–900.

Mégard, F., Noble, D.C., McKee, E.H., Bellon, H., 1984. Multiple pulses of Neogene compressive deformation in the Ayacucho intermontane basin, Andes of central Peru. Geol. Soc. Am. Bull. 95, 1108–1117.

Meisling, K.E., Cobbold, P.R., Mount, V.S., 2001. Segmentation of an obliquely rifted margin, Campos and Santos basins, southeastern Brazil. American Association of Petroleum Geologists Bulletin 85 (11), 1903–1924.

Mohriak, W. U., Rabelo, J. L., De Matos, R. D., De Barros, M. C., 1995. Deep seismic reflection profiling of sedimentary basins offshore Brazil: Geological objectives and preliminary results in the Sergipe Basin. Journal of Geodynamics, 20**,** 515-539.

Mohriak, W., Nemčok, M., Enciso, G., 2008. South Atlantic divergent margin evolution: rift-border uplift and salt tectonics in the basins of SE Brazil. Geological Society, London, Special Publications, 294**,** 365-398.

Mohriak, W. U., Palagi, P. R., Mello, M. R., 1998. Tectonic evolution of south Atlantic salt basins: AAPG Bull., v.82, no.10, p. 1945.

Mohriak, W.U., 2003. Bacias sedimentares da margem continental Brasileira. In: Bizzi, L.A., Schobbenhaus, C., Vidotti, R.M., Goncalves, J.H. (Eds.), Geologia, Tectonica e Recursos Minerais do Brasil. CPRM, Brasilia, pp. 87-165.

Moreira, J.L., Carminatti, M., 2004. Eocene slope and basin depositional systems in the Santos Basin. Bol. Geociênc. Petrobras 12, 73–87.

Morley, C.K., 2002. Evolution of large normal faults: evidence from seismic reflection data. AAPG Bull. 86, 961–978.

Morley, C. K. 1999. Patterns of displacement along large normal faults: implications for basin evolution and fault propagation, based on examples from east Africa. AAPG bulletin, 83, 613-634.

Ojeda, H., 1982. Structural framework, stratigraphy, and evolution of Brazilian marginal basins. AAPG Bulletin, 66**,** 732-749.

Peacock, D.C.P., 2002. Propagation, interaction and linkage in normal fault systems. Earth Sci. Rev. 58, 121–142.

Peacock, D.C.P., Sanderson, D.J., 1991. Displacements, segment linkage and relay ramps in Normal fault zones. Journal of Structural Geology. 13, 721–733.

Penge, J., Munns, J.W., Taylor, B., Windle, T.M.F., 1999. Rift–raft tectonics: examples of gravitational tectonics from the Zechstein basins of northwest Europe. Geological Society, London, Petroleum Geology Conference series 5, 201-213.

Piedade, A., Alves, T. M., 2017. Structural styles of Albian rafts in the Espírito Santo Basin (SE Brazil): Evidence for late raft compartmentalisation on a 'passive' continental margin. Marine and Petroleum Geology 79, pp. 201-221.

Pilcher, R.S., Murphy, R.T., Ciosek, J.M., 2014. Jurassic raft tectonics in the northeastern Gulf of Mexico. Interpretation 2, SM39-SM55.

Plummer, P. S. and Gostin, V. A. 1981. Shrinkage cracks: desiccation or syneresis. Journal of Sedimentary Petrology 51, 1147-1156.

Richard, P., Krantz, R.W., 1991. Experiments on fault reactivation in strike-slip mode. Tectonophysics 188 (1-2), 117–131.

Stewart, S.A., 2001. Displacement distributions on extensional faults: implications for fault stretch, linkage, and seal. AAPG Bull. 85, 587–600.

Tao, Z., Alves, T.M., 2019. Impacts of data sampling on the interpretation of normal fault propagation and segment linkage. Tectonophysics, 762, 79-96.

Vendeville, B.C., 2005. Salt tectonics driven by sediment progradation: Part I—Mechanics and kinematics. AAPG Bulletin 89, 1071-1079.

Viana, A., Figueiredo, A., Faugeres, J.-C., Lima, A., Gonthier, E., Brehme, I., Zaragosi, S., 2003. The Sao Tomé deep-sea turbidite system (southern Brazil Basin): Cenozoic Seismic stratigraphy and sedimentary processes. AAPG Bull. 87, 873–894.

Vieira, P. E., Bruhn, C. H. L., Santos, C. F., Del Rey, A. C., Alves, R. G., 2007. Golfinho Field-Discovery, Development, and Future Prospects. Offshore Technology Conference.

Walsh, J.J., Watterson, J., 1989. Displacement gradients on fault surfaces. Journal of Structural Geology. 11, 307–316.

Zhang, L., Luo, X., Vasseur, G., Yu, C., Yang, W., Lei, Y., Song, C., Yu, L., Yan, J., 2011. Evaluation of geological factors in characterizing fault connectivity during hydrocarbon migration: application to the Bohai Bay Basin. Mar. Pet. Geol. 28, 1634–1647.

Figure captions

Fig. 1. (a) Map of the southeast Brazilian margin showing the location of the study area (Espírito Santo Basin (BES-100)). b) Two-Way Travel time (TWTT) structural map of the sea floor highlighting features such as submarine slope channels running parallel to the bathymetric slope.

Fig. 2. Seismic-stratigraphic correlation between the interpreted post-rift seismic units and stratigraphic ages, tectonic phases/megasequences and unconformities related to regional tectonic events in the upper slope (extensional) region of the Espírito Santo Basin (modified from França et al., 2007). Velocity information taken from Alves (2012). Deformation episodes in central Andes are based on Mégard (1984) and Gregory-Wodzicki (2000).

Fig. 3. a) Uninterpreted, and b) Interpreted seismic section across the study area. The section highlights the large roller faults bounding Cretaceous minibasins, normal faults over rollover anticlines, withdrawal synclines adjacent to roller fault and diapir, tectonic rafts between and above salt structures. Tectonic raft 2 forms the core of wide rollover anticlines. Tier 1, 2 and 3 faults dominantly cross-cut horizons H4, H5 and H6 respectively. Salt rollers, diapirs and tectonic rafts occur in Units S2 and S3.

Fig. 4. a) Uninterpreted, and b) Interpreted seismic section across the study area. The section highlights large roller faults bounding Cretaceous minibasins, normal faults over rollover anticlines, drag folds adjacent to roller faults, tectonic rafts between and above salt rollers and local reactivated pop-up structures. Tectonic raft 2 forms the core of rollover anticlines. Tier 1, 2 and 3 faults dominantly cross-cut horizons H4, H5 and H6 respectively. The presence of reactivated pop-up structures in Paleogene strata (Unit S6), and the drag folds adjacent to the roller fault, materialise the diachronous grounding of tectonic rafts.

Fig. 5. a) TWTT structural map of Horizon H4, showing distribution of fault families in the study area; b) Interpreted sketch highlighting the geometry of fault families and the N-S strike of wide rollover anticlinal zones (grey panel) sub-parallel to the strike of tectonic raft 2.

Fig. 6. a) TWTT structural map of horizon H3; b) Interpreted sketch highlighting the geometry of N-S trending tectonic rafts separated by salt minibasins. Tectonic raft 2 forms the core of rollover anticlines in the study area.

Fig. 7. TWTT structural maps for representative intervals in the study area highlighting variations in the geometry of distinct fault tiers over rollover anticlines (i.e., spacings, orientation, intersection relationships and linearity of fault segments). a) Tier 1 faults show curved polygonal plan-view geometries, b) Tier 2 faults show rectangular polygonal plan-view geometries, and c) Tier 3 faults show irregular polygonal geometries in plan view.

Fig. 8. TWTT structural map and interpreted sketch highlighting the geometry of distinct fault tiers over N-S trending rollover anticlines (grey panel). a) Tier 1 faults: curved polygonal pattern, b) Tier 2 faults: rectangular polygonal pattern, and c) Tier 3 faults: irregular polygonal pattern.

Fig. 9. a) Representative vertical throw-depth (T-Z) plots of Tier 1 faults, b) Throw contour map of the Tier 1 faults showing throw distributions and, c) Throw-distance (T-X) plots through the contour map (see Fig. 9b for profile lines location). Throw maxima A, B and C are individual segments of pre-existing faults, separated by throw minima. H4, S4 and S5 relate to main horizons and seismic units.

Fig. 10. a) Representative vertical throw-depth (T-Z) plots of Tier 2 faults, b) Throw contour map of the Tier 2 faults showing throw distributions and, c) Throw-distance (T-X) plots through the

contour map (see Fig. 10b for profile lines location). Throw maxima A, B and C are individual segments of pre-existing faults, separated by throw minima. H4, H5, and H6 are horizons while S5, S6 and S7 are seismic units.

Fig. 11. a) Representative of vertical throw-depth (T-Z) plots of Tier 3 faults, b) Throw contour map of the Tier 3 faults showing throw distributions and, c) Throw-distance (T-X) plots through the contour map (see Fig. 11b for profile lines location). Throw maxima A, B and C are individual segments of pre-existing faults, separated by throw minima. H5 and H6 are horizons while S6 and S7 are seismic units.

Fig. 12. a) and c) Representative vertical throw-depth (T-Z) plots for seaward- and landward-dipping roller faults. H4, H5 and H6 are horizons while S4, S5, S6 and S7 are seismic units, b) and d) Throw-depth (T-Z) contour maps of roller faults showing their corresponding throw distributions.

Fig. 13. Schematic illustration of the relative age and time-span of distinct fault tiers mapped over a N-S trending rollover anticlines that are sub-parallel to tectonic raft 2. Plotted in the diagram is the number of reflections above and below main unconformities related to regional tectonic episodes in the Espirito Santo basin. Tier 1, 2 and 3 faults dominantly cross-cut Campanian (H4), Paleocene (H5) and Pre-Upper Eocene (H6) unconformities respectively. S2 to S7 are interpreted seismic units.

Fig. 14. Schematic model for the development of rollover anticlines and associated normal faults.

Fig. 15. Schematic model explaining the gravitational gliding of tectonic rafts and their relationship with local structures (listric faults, rollover anticlines and normal faults. Figure is modified from Duval et al. (1992).

Table caption

Table 1. Summary of statistical data on the distinct fault tiers formed over rollover anticlines.

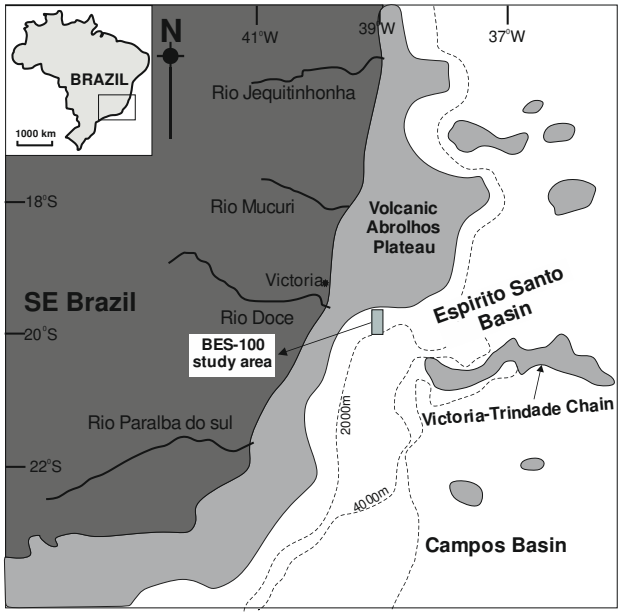
BRAZIL
1000 km
N
41°W
39°W
37°W
Rio Jequitinhonha
18°S
Rio Mucuri
Volcanic
Abrolhos
Plateau
Victoria
SE Brazil
Rio Doce
Espirito Santo
Basin
20°S
BES-100
study area
Victoria-Trindade Chain
2000m
Rio Paralba do sul
22°S
4000m
Campos Basin

Fig. 1.

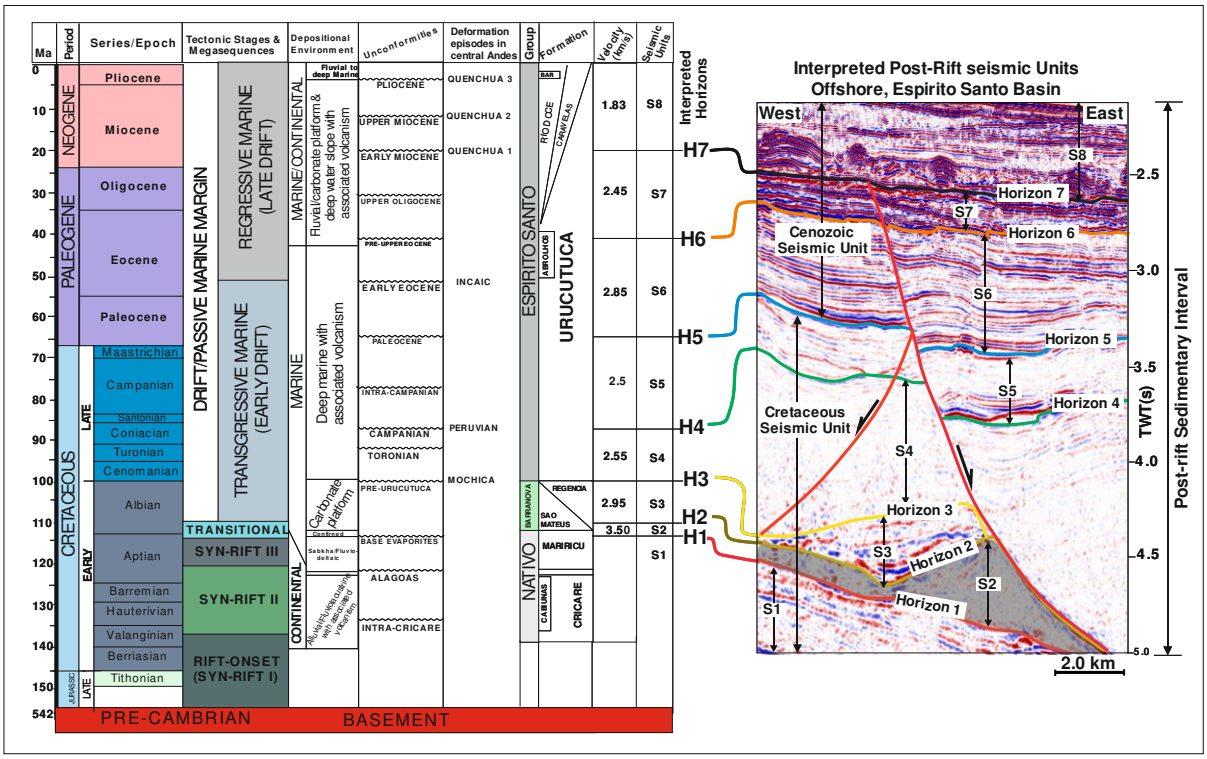
Interpreted Post-Rift seismic Units
Offshore, Espirito Santo Basin
West
East
Cenozoic
Seismic Unit
Cretaceous
Seismic Unit
Horizon 7
Horizon 6
Horizon 5
Horizon 4
Horizon 3
Horizon 2
Horizon 1
S8
S7
S6
S5
S4
S3
S2
S1
H7
H6
H5
H4
H3
H2
H1
2.0 km
TWT(s)
Post-rift Sedimentary Interval
Ma
Period
Series/Epoch
Tectonic Stages & Megasequences
Depositional Environment
Unconformities
Deformation episodes in central Andes
Group
Formation
Velocity (km/s)
Seismic Units
Interpreted Horizons
NEOGENE
PALEOGENE
CRETACEOUS
JURASSIC
Pliocene
Miocene
Oligocene
Eocene
Paleocene
Maastrichian
Campanian
Santonian
Coniacian
Turonian
Cenomanian
Albian
Aptian
Barremian
Hauterivian
Valanginian
Berriasian
Tithonian
DRIFT/PASSIVE MARINE MARGIN
REGRESSIVE MARINE (LATE DRIFT)
TRANSGRESSIVE MARINE (EARLY DRIFT)
TRANSITIONAL
SYN-RIFT III
SYN-RIFT II
RIFT-ONSET (SYN-RIFT I)
MARINE/CONTINENTAL
MARINE
CONTINENTAL
Fluvial to deep Marine
Fluvial/carbonate platform & deep water slope with associated volcanism
Deep marine with associated volcanism
Carbonate platform
PLIOCENE
UPPER MIOCENE
EARLY MIOCENE
UPPER OLIGOCENE
PRE-UPPER EOCENE
EARLY EOCENE
PALEOCENE
INTRA-CAMPANIAN
CAMPANIAN
TORONIAN
PRE-URUCUTUCA
BASE EVAPORITES
ALAGOAS
INTRA-CRICARE
QUENCHUA 3
QUENCHUA 2
QUENCHUA 1
INCAIC
PERUVIAN
MOCHICA
ESPIRITO SANTO
BARRA VELHA
ABROLHOS
URUCUTUCA
BARREMIANA
REGENCIA
SAO MATEUS
NATIVO
MARIRICU
CABIUNAS
CRICARE
1.83
2.45
2.85
2.5
2.55
2.95
3.50
S8
S7
S6
S5
S4
S3
S2
S1
PRE-CAMBRIAN
BASEMENT

Fig. 2.

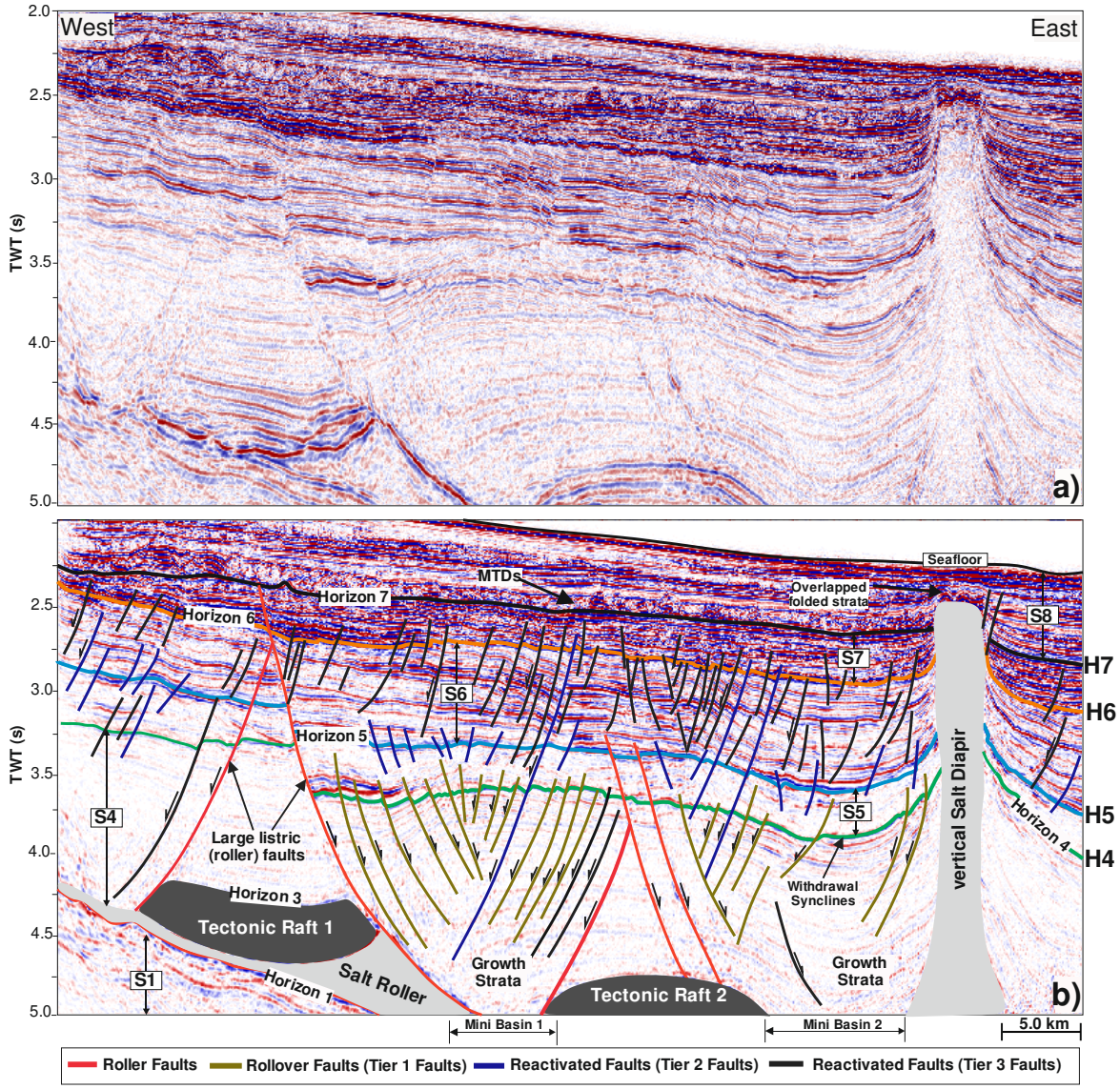
West
East
a)
TWT (s)
2.0
2.5
3.0
3.5
4.0
4.5
5.0
MTDs
Horizon 7
Horizon 6
Horizon 5
Horizon 4
Horizon 3
Horizon 1
Seafloor
Overlapped folded strata
S1
S4
S5
S6
S7
S8
H7
H6
H5
H4
Large listric (roller) faults
Tectonic Raft 1
Tectonic Raft 2
Salt Roller
Growth Strata
Growth Strata
Withdrawal Synclines
vertical Salt Diapir
Mini Basin 1
Mini Basin 2
5.0 km
b)
Roller Faults
Rollover Faults (Tier 1 Faults)
Reactivated Faults (Tier 2 Faults)
Reactivated Faults (Tier 3 Faults)

Fig. 3.

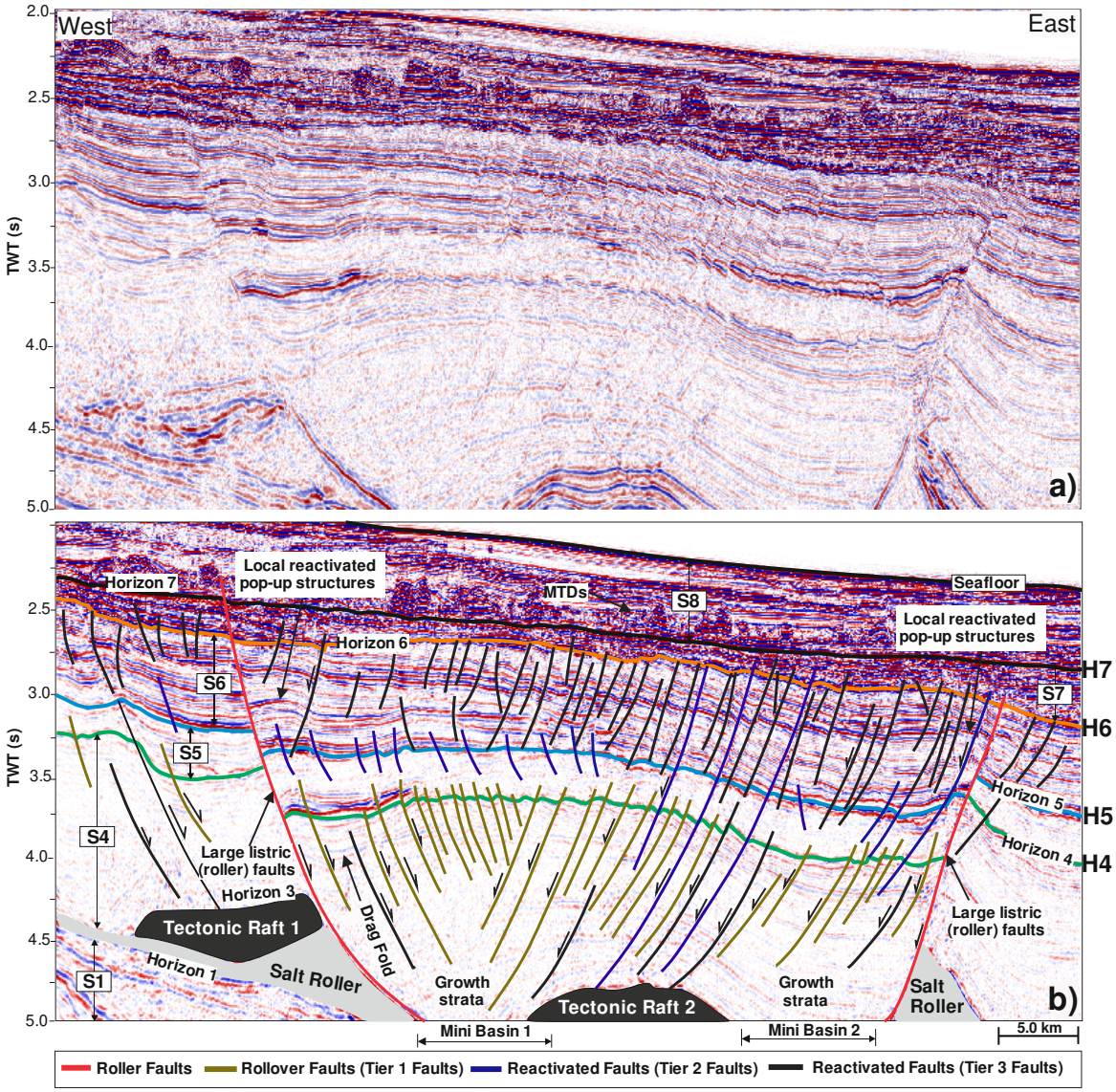
West
East
a)
TWT (s)
2.0
2.5
3.0
3.5
4.0
4.5
5.0
Horizon 7
Local reactivated pop-up structures
MTDs
S8
Seafloor
Local reactivated pop-up structures
Horizon 6
S6
S7
H7
H6
S5
Horizon 5
H5
S4
Large listric (roller) faults
Horizon 4
H4
Horizon 3
Tectonic Raft 1
Drag Fold
Large listric (roller) faults
Horizon 1
Salt Roller
Growth strata
Tectonic Raft 2
Growth strata
Salt Roller
S1
b)
Mini Basin 1
Mini Basin 2
5.0 km
Roller Faults
Rollover Faults (Tier 1 Faults)
Reactivated Faults (Tier 2 Faults)
Reactivated Faults (Tier 3 Faults)

Fig. 4.

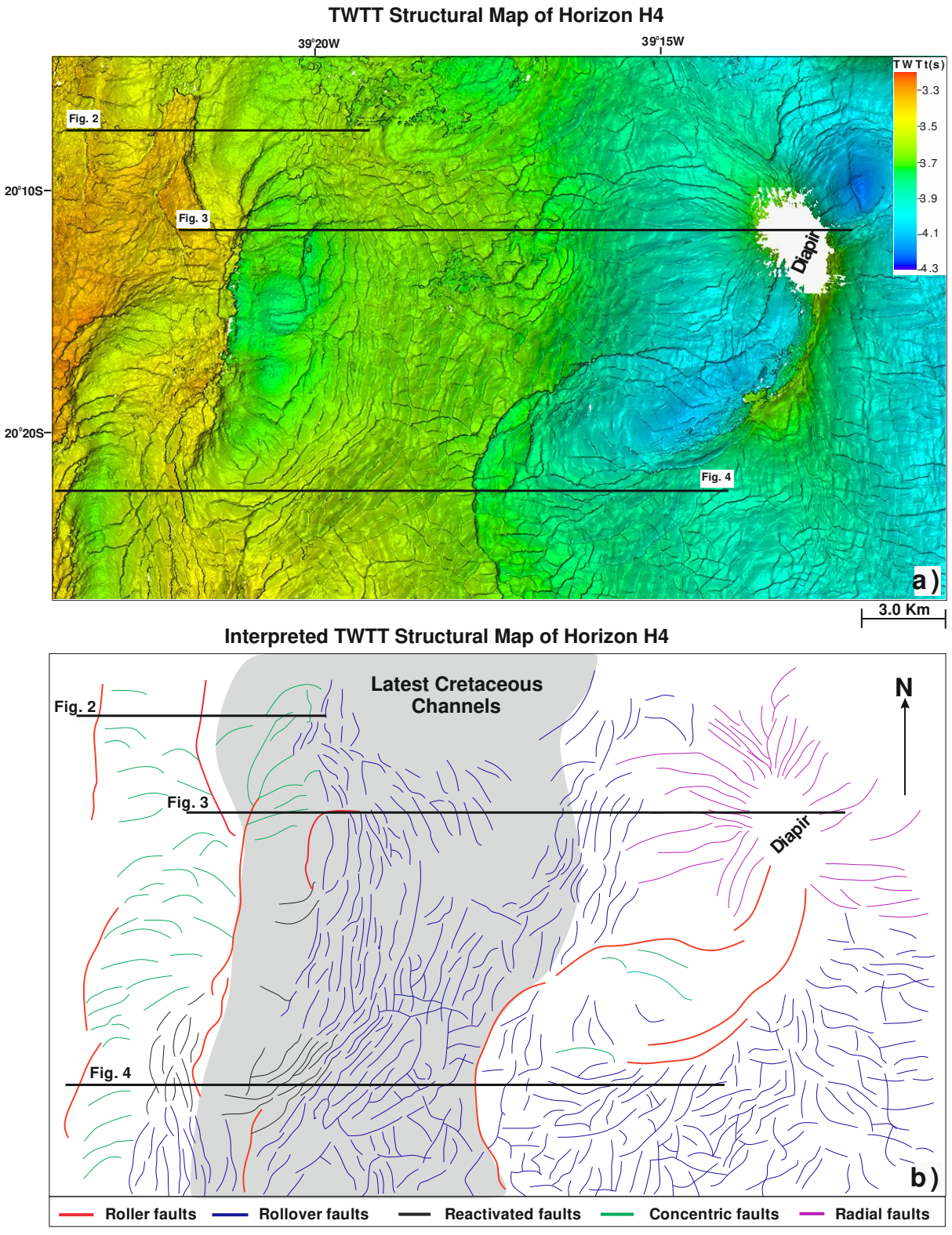
TWTT Structural Map of Horizon H4
39°20W
39°15W
20°10S
20°20S
Fig. 2
Fig. 3
Fig. 4
Diapir
TWTT(s)
3.3
3.5
3.7
3.9
4.1
4.3
a)
3.0 Km
Interpreted TWTT Structural Map of Horizon H4
Latest Cretaceous Channels
N
Fig. 2
Fig. 3
Fig. 4
Diapir
b)
Roller faults
Rollover faults
Reactivated faults
Concentric faults
Radial faults

Fig. 5.

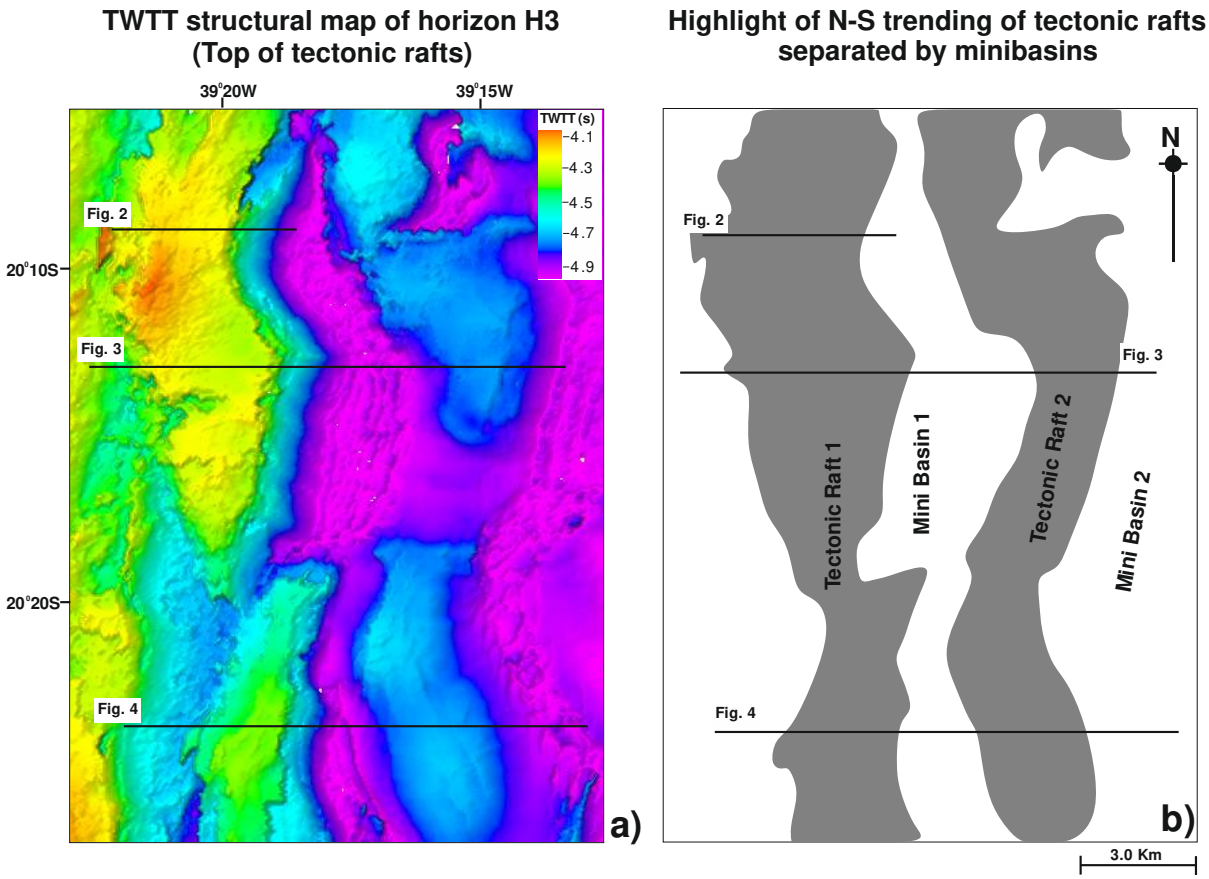
TWTT structural map of horizon H3
(Top of tectonic rafts)
39°20W
39°15W
20°10S
20°20S
TWTT (s)
-4.1
-4.3
-4.5
-4.7
-4.9
Fig. 2
Fig. 3
Fig. 4
a)
Highlight of N-S trending of tectonic rafts
separated by minibasins
N
Fig. 2
Fig. 3
Fig. 4
Tectonic Raft 1
Mini Basin 1
Tectonic Raft 2
Mini Basin 2
b)
3.0 Km

Fig. 6.

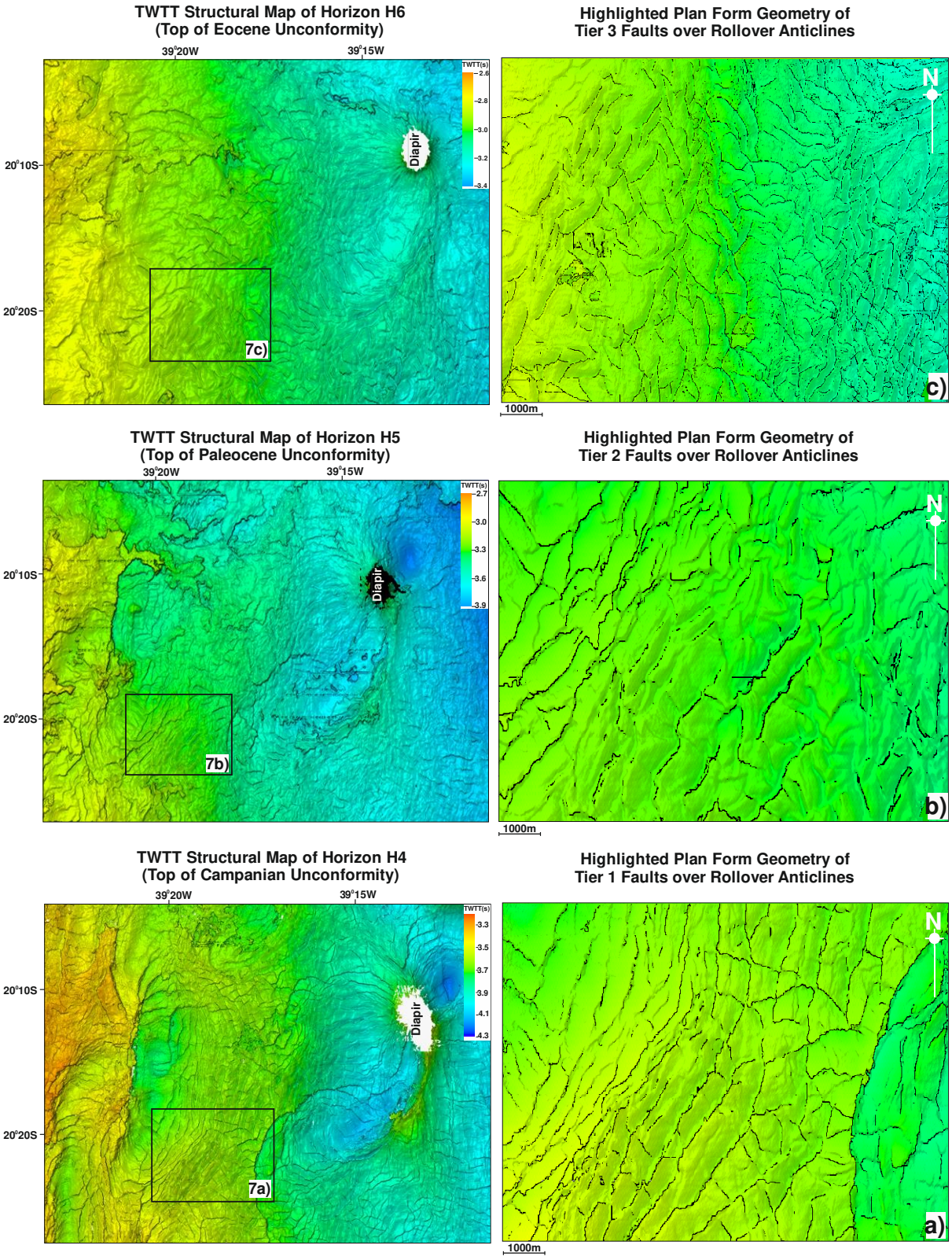
TWTT Structural Map of Horizon H6
(Top of Eocene Unconformity)
39°20W
39°15W
20°10S
20°20S
TWTT(s)
-2.6
-2.8
-3.0
-3.2
-3.4
Diapir
7c)
Highlighted Plan Form Geometry of
Tier 3 Faults over Rollover Anticlines
N
c)
1000m
TWTT Structural Map of Horizon H5
(Top of Paleocene Unconformity)
39°20W
39°15W
20°10S
20°20S
TWTT(s)
-2.7
-3.0
-3.3
-3.6
-3.9
Diapir
7b)
Highlighted Plan Form Geometry of
Tier 2 Faults over Rollover Anticlines
N
b)
1000m
TWTT Structural Map of Horizon H4
(Top of Campanian Unconformity)
39°20W
39°15W
20°10S
20°20S
TWTT(s)
-3.3
-3.5
-3.7
-3.9
-4.1
-4.3
Diapir
7a)
Highlighted Plan Form Geometry of
Tier 1 Faults over Rollover Anticlines
N
a)
1000m

Fig. 7.

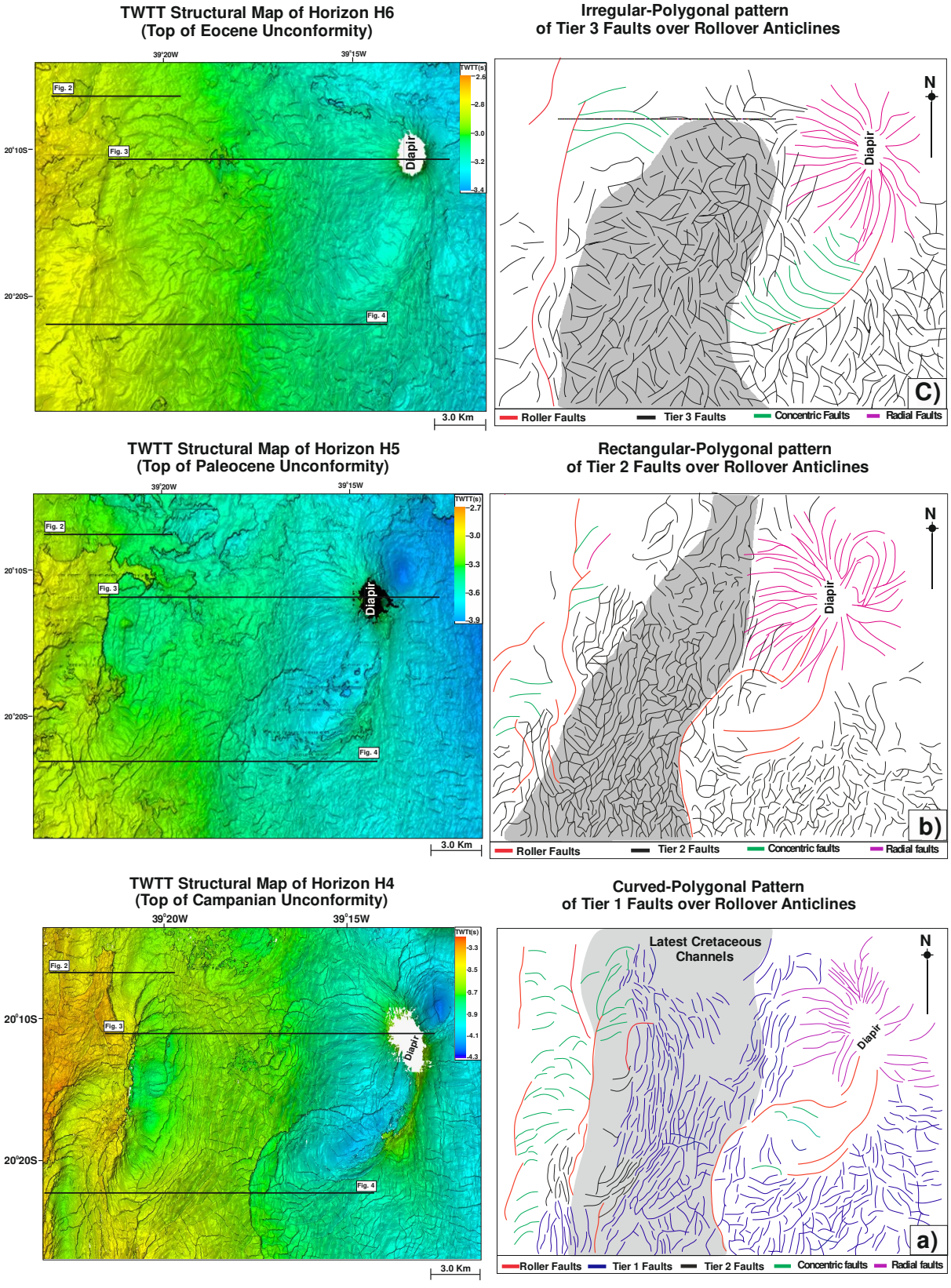
TWTT Structural Map of Horizon H6
(Top of Eocene Unconformity)
Irregular-Polygonal pattern
of Tier 3 Faults over Rollover Anticlines
TWTT Structural Map of Horizon H5
(Top of Paleocene Unconformity)
Rectangular-Polygonal pattern
of Tier 2 Faults over Rollover Anticlines
TWTT Structural Map of Horizon H4
(Top of Campanian Unconformity)
Curved-Polygonal Pattern
of Tier 1 Faults over Rollover Anticlines
39°20W
39°15W
20°10S
20°20S
Fig. 2
Fig. 3
Fig. 4
Diapir
TWTT(s)
3.0 Km
N
Latest Cretaceous
Channels
C)
b)
a)
Roller Faults
Tier 1 Faults
Tier 2 Faults
Tier 3 Faults
Concentric Faults
Concentric faults
Radial Faults
Radial faults

Fig. 8.

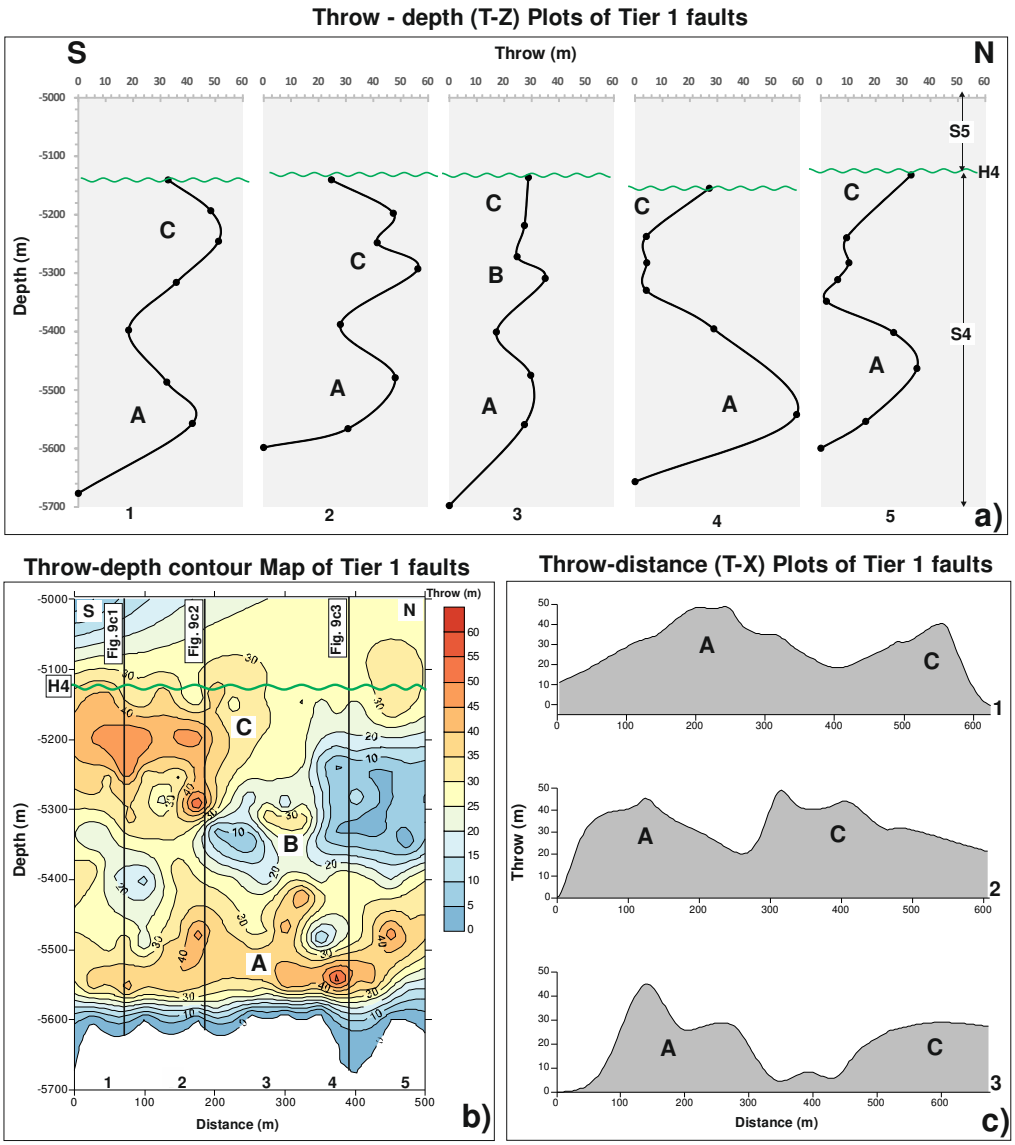
Throw - depth (T-Z) Plots of Tier 1 faults
S
N
Throw (m)
Depth (m)
S5
H4
S4
A
B
C
1
2
3
4
5
a)
Throw-depth contour Map of Tier 1 faults
Fig. 9c1
Fig. 9c2
Fig. 9c3
Distance (m)
b)
Throw-distance (T-X) Plots of Tier 1 faults
c)

Fig. 9.

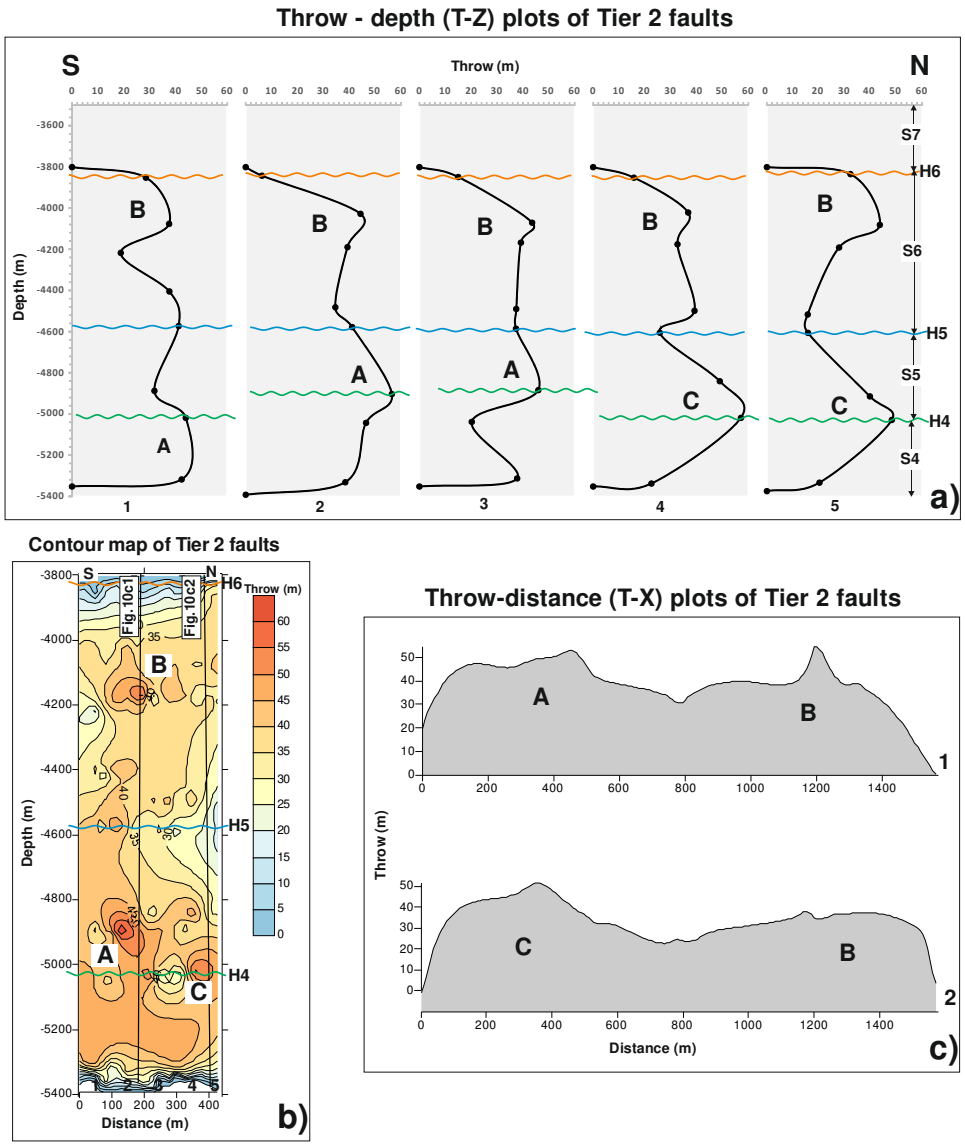
Throw - depth (T-Z) plots of Tier 2 faults
S
N
Throw (m)
Depth (m)
S7
H6
S6
H5
S5
H4
S4
a)
Contour map of Tier 2 faults
Fig. 10c1
Fig. 10c2
Throw (m)
Distance (m)
b)
Throw-distance (T-X) plots of Tier 2 faults
Throw (m)
Distance (m)
c)

Fig. 10.

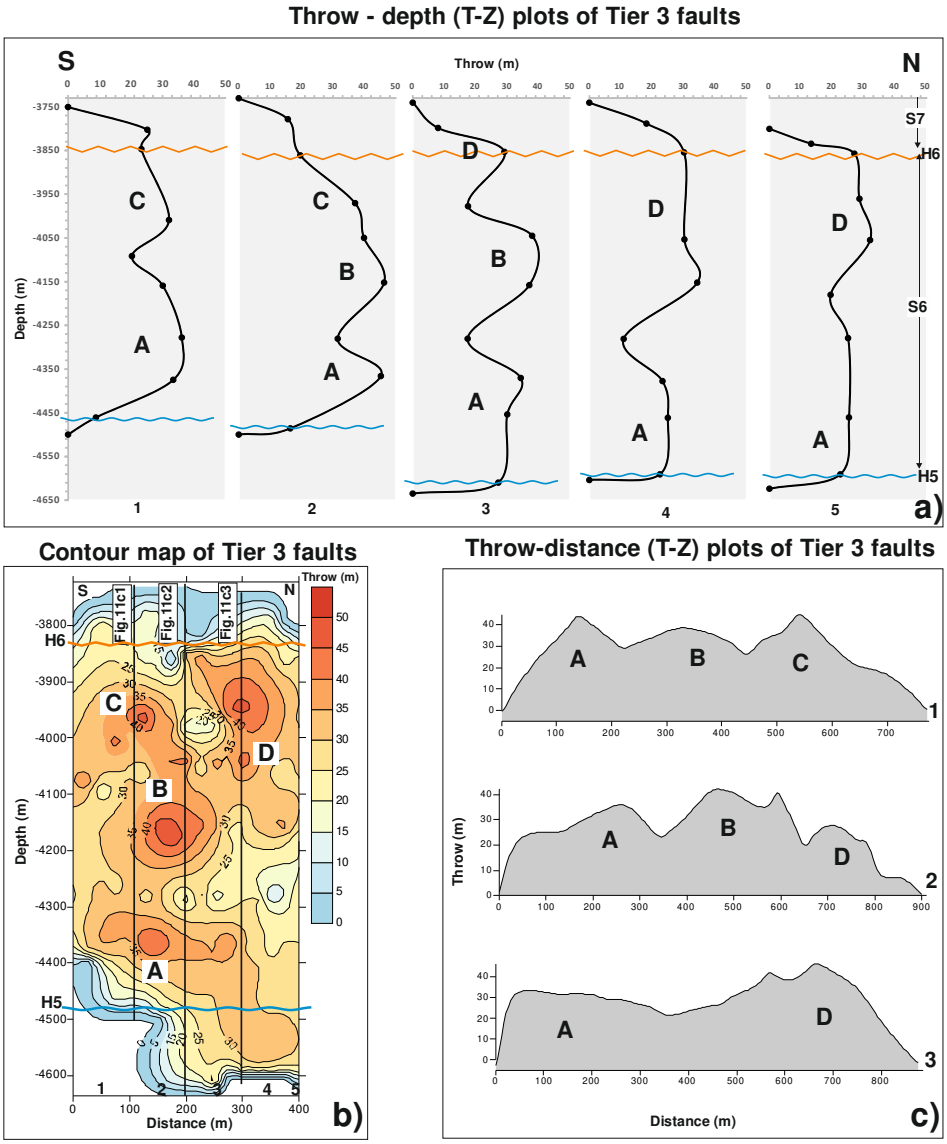
Throw - depth (T-Z) plots of Tier 3 faults
S
N
Throw (m)
Depth (m)
S7
H6
S6
H5
A
B
C
D
1
2
3
4
5
a)
Contour map of Tier 3 faults
Fig.11c1
Fig.11c2
Fig.11c3
Distance (m)
b)
Throw-distance (T-Z) plots of Tier 3 faults
Throw (m)
Distance (m)
c)

Fig. 11.

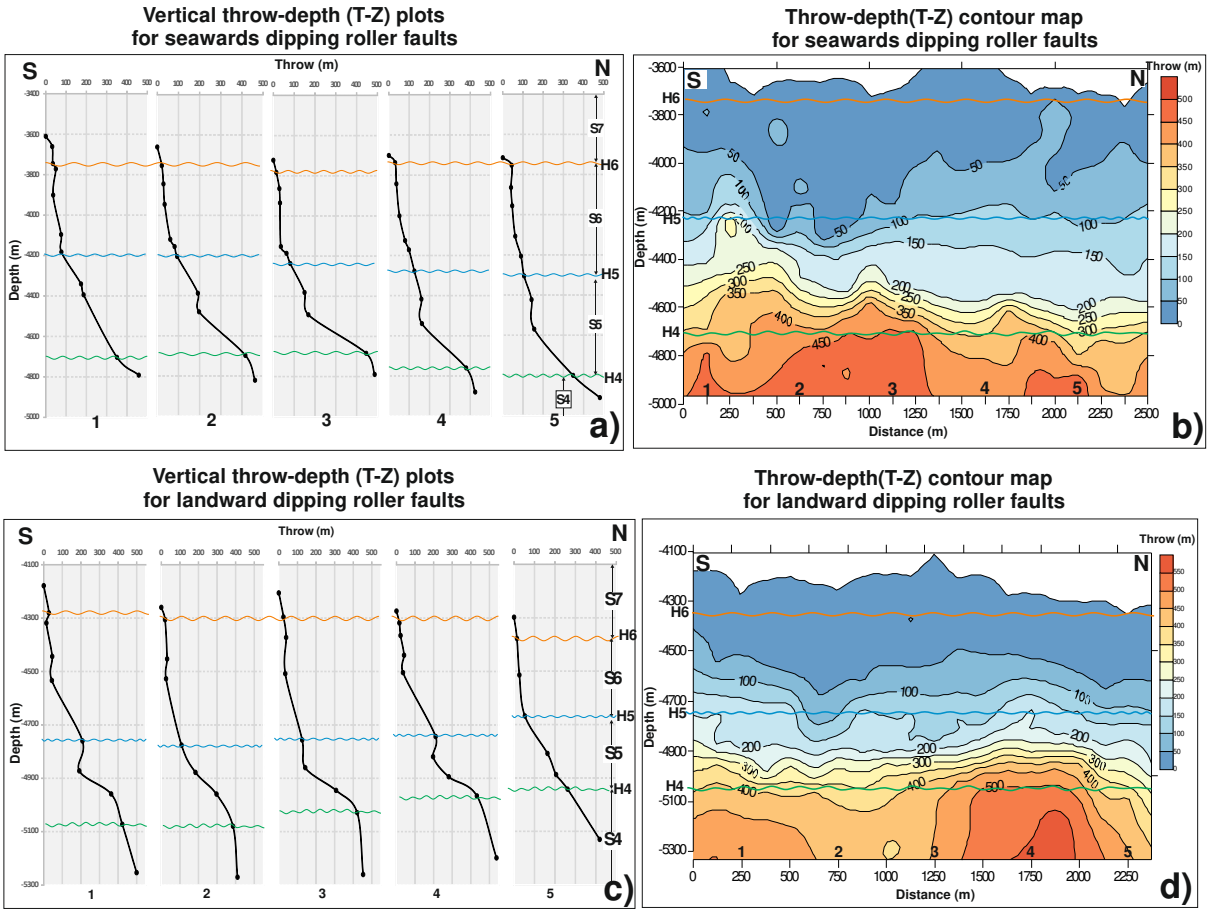
Vertical throw-depth (T-Z) plots
for seawards dipping roller faults
Throw-depth(T-Z) contour map
for seawards dipping roller faults
Vertical throw-depth (T-Z) plots
for landward dipping roller faults
Throw-depth(T-Z) contour map
for landward dipping roller faults
Throw (m)
Depth (m)
Distance (m)
S
N
H4
H5
H6
S4
S5
S6
S7
a)
b)
c)
d)

Fig. 12.

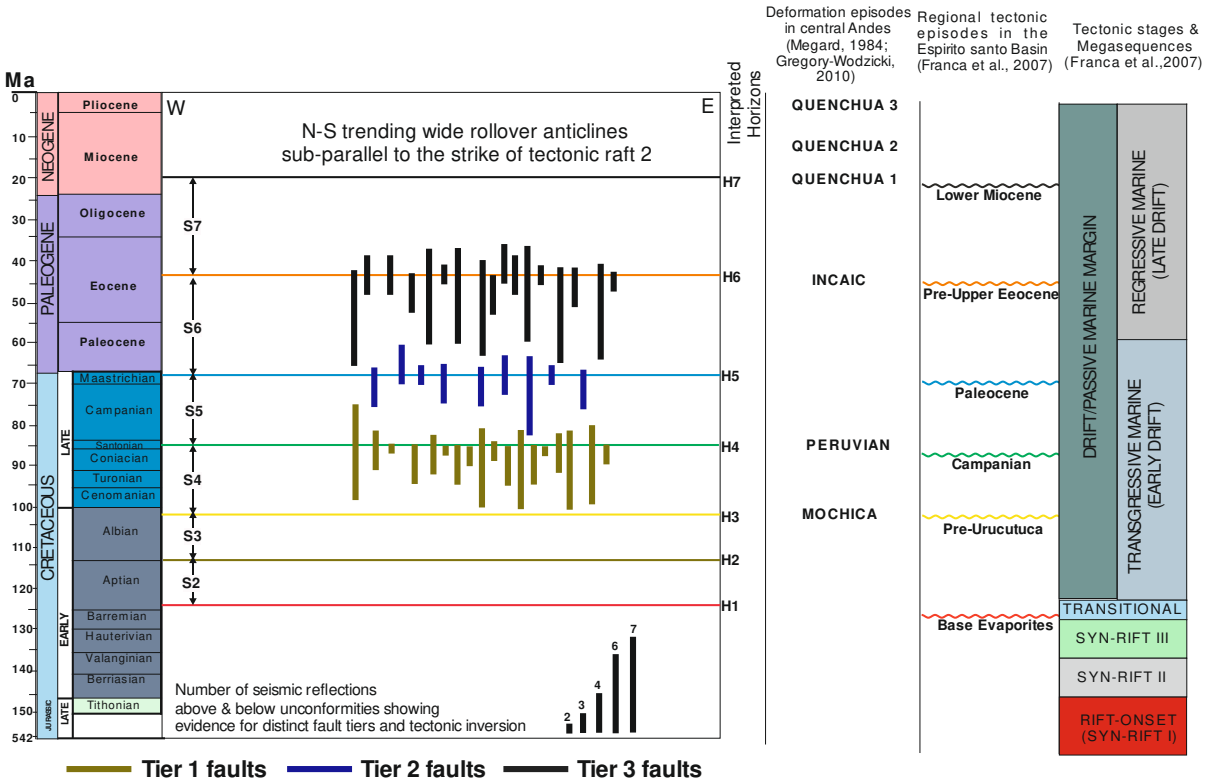
Ma
NEOGENE
PALEOGENE
CRETACEOUS
Pliocene
Miocene
Oligocene
Eocene
Paleocene
Maastrichian
Campanian
Santonian
Coniacian
Turonian
Cenomanian
Albian
Aptian
Barremian
Hauterivian
Valanginian
Berriasian
Tithonian
LATE
EARLY
W
E
N-S trending wide rollover anticlines
sub-parallel to the strike of tectonic raft 2
Interpreted Horizons
H1
H2
H3
H4
H5
H6
H7
S2
S3
S4
S5
S6
S7
Number of seismic reflections
above & below unconformities showing
evidence for distinct fault tiers and tectonic inversion
Tier 1 faults
Tier 2 faults
Tier 3 faults
Deformation episodes in central Andes (Megard, 1984; Gregory-Wodzicki, 2010)
QUENCHUA 3
QUENCHUA 2
QUENCHUA 1
INCAIC
PERUVIAN
MOCHICA
Regional tectonic episodes in the Espirito santo Basin (Franca et al., 2007)
Lower Miocene
Pre-Upper Eeocene
Paleocene
Campanian
Pre-Urucutuca
Base Evaporites
Tectonic stages & Megasequences (Franca et al.,2007)
DRIFT/PASSIVE MARINE MARGIN
REGRESSIVE MARINE (LATE DRIFT)
TRANSGRESSIVE MARINE (EARLY DRIFT)
TRANSITIONAL
SYN-RIFT III
SYN-RIFT II
RIFT-ONSET (SYN-RIFT I)

Fig. 13.

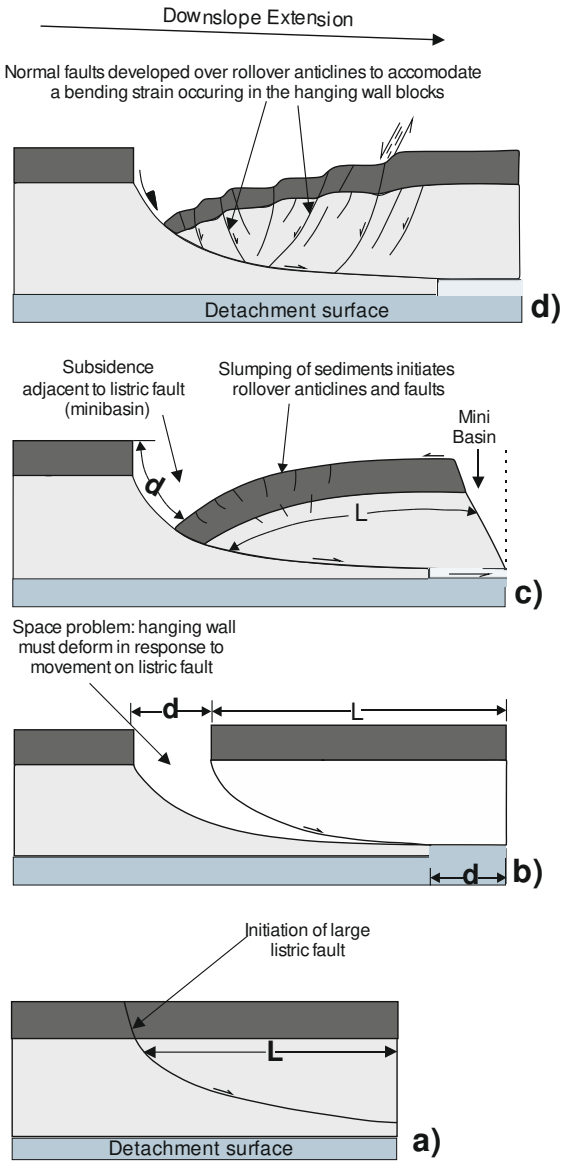
Downslope Extension
Normal faults developed over rollover anticlines to accomodate a bending strain occuring in the hanging wall blocks
Detachment surface
d)
Subsidence adjacent to listric fault (minibasin)
Slumping of sediments initiates rollover anticlines and faults
Mini Basin
d
L
c)
Space problem: hanging wall must deform in response to movement on listric fault
d
L
d
b)
Initiation of large listric fault
L
Detachment surface
a)

Fig. 14.

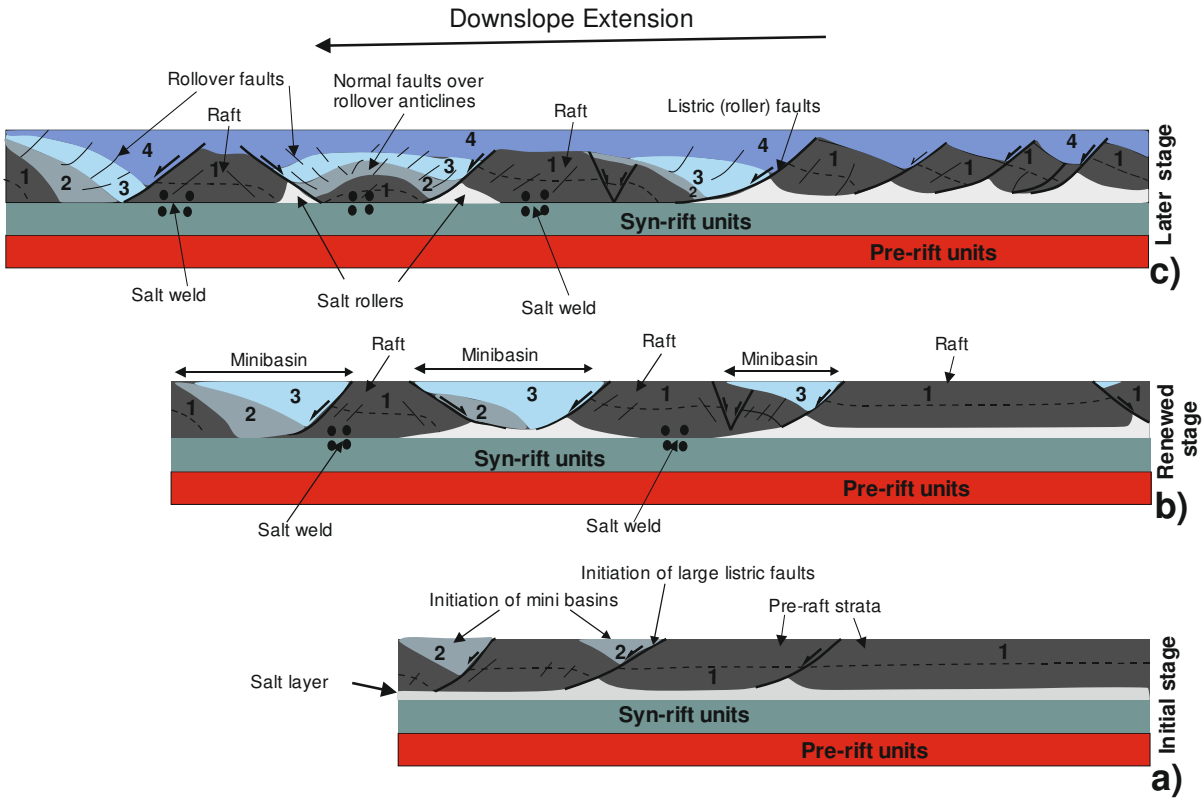
Downslope Extension
Rollover faults
Raft
Normal faults over rollover anticlines
Raft
Listric (roller) faults
Syn-rift units
Pre-rift units
Salt weld
Salt rollers
Salt weld
Later stage
c)
Minibasin
Raft
Minibasin
Raft
Minibasin
Raft
Syn-rift units
Pre-rift units
Salt weld
Salt weld
Renewed stage
b)
Initiation of large listric faults
Initiation of mini basins
Pre-raft strata
Salt layer
Syn-rift units
Pre-rift units
Initial stage
a)

Fig. 15.

Table 1.

Fault families	Maximum length (m)	Minimum length (m)	Average length (m)	Average spacing (m)	Maximum Throw (m)	Average Throw (m)
Rollover faults (Tier 1)	620	220	410	250	58	47
Reactivated faults (Tier 2)	650	280	430	310	55	48
Reactivated faults (Tier 3)	550	120	390	210	50	46
Roller faults	12,522	5,340	8,560	4,500	530	470
Concentric faults	4,562	1,860	2,650	1,250	54	50